Channel Response and Target Detection in Shallow Water

by

Wenhua Li

Submitted to the Department of Ocean Engineering in partial fulfillment of the requirements for the degree of

Master of science

at the

MASSACHUSETTS INSTITUTE OF TECHNOLOGY

February 1,1996

Author .....
Department of Ocean Engineering
Sept 30, 1995

Certified by .....
Assistant Prof. Robert Fricke
Ocean Engineering
Thesis Supervisor

Accepted by .....
A. Douglas Carmichael
Chairman, Departmental Graduate Committee
Department of Ocean Engineering

Channel Response and Target Detection in Shallow Water

by

Wenhua Li

Submitted to the Department of Ocean Engineering on Sept. 30, 1995, in partial fulfillment of the requirements for the degree of Master of Science in Ocean Engineering.

Abstract

This thesis presents the design, simulation and testing on real data of a signal processing system for use in a highly reverberant shallow water environment. The system applies a combination of homomorphic deconvolution and Wiener filter to recover the transmitted signal and increase the resolution of the channel impulse response. Based on the high resolution channel response, the target distribution is presented using a B-scan map with target localization based on multi-aspect arrival processing. Excess path length due to multipath is estimated and is beneficial in removing the spurious detections caused by the multipath. Since the system assimilates the advantages of both complex cepstrum and Wiener filter, it is independent of the transmitted signal and the transfer function, and robust to ambient noise. Therefore, it is capable of coping with more realistic propagation conditions where, in general, the various signal arrivals have a complex mixed-phase structure. The efficiency of the method is demonstrated by both simulated and real reverberation data in shallow water.

Thesis Supervisor: J. Robert Fricke
Title: Assistant Professor

Acknowledgments

First and foremost I would like to thank Professor Robert Fricke for advising me as a Master student. Professor Robert Fricke, your inspirational advice and strict attitude toward research give me a deep impression. Without your consideration and encouragement, it would be difficult for me to produce this thesis. Thank you with all my sincerity.

Thanks to the Draper Laboratories for the support and funding. Thanks to my parents for their endless encouragement and love. Thanking all those who have contributed in some way to help me get through the days in my first year at MIT.

Thanks from the bottom of my heart to my husband for his support and understanding. Xiangzhou, you have really made my life complete and I look forward to stand with you through thick and thin.

Contents

List of Figures

List of Tables

Chapter 1

Introduction

For many economic and military reasons, there are abundant interests in shallow water characteristics. However, because of the highly variable sea condition and the complex propagation structure such as surface reflection, bottom reflection or refraction, and volume refraction, it is extremely difficult in shallow water to remove the effects of multipaths and obtain useful information from experimental data in order to develop practical systems for target detection and communication.

The aim of this thesis is to provide a powerful method, which uses a combination of complex cepstrum and Wiener filter[1] to improve the resolution of channel response estimation. This method is used to remove the effects of multipath and find the true underwater targets.

In this thesis, the received signal is modeled as the convolution of a transmitted signal with the channel response plus additive white noise. In real life, the channel response, the additive noise, and even the transmitted signal, are not minimum phase signals, which is the assumption for conventional application of a Wiener filter[2-4]. Thus, it is necessary to use homomorphic deconvolution[5] to factorize the received signal into minimum and maximum phase components through which we can determine the parameters of the causal and anticausal Wiener filters with the deconvolved wavelet. Then the channel response with high resolution can be obtained by using the received signal as the input of the constructed Wiener filter (Figure 2.2). The 'B-scan map' and 'target localization' are used to get the target spatial distribution based on the sharpened channel response, which gives an intuition of the potential targets. The 'excess path length due to multipath' can

also be successfully obtained from the channel response while it seems impossible to get from the original signal. This result is encouraging because the multipath structure can be considered as a space filter to the received data in finding the true echo from an object. Besides, theoretically, the shape of 'the excess path' curves is determined by the ocean environmental parameters. It implies that if these curves can be achieved from the experimental data, we might be able to invert the key parameters and then obtain some useful information about the ocean environment.

In chapter 2, the complex cepstrum, the Wiener filter and their combination are discussed theoretically. The simulation results and their analysis are presented in Chapter 3. Results with experimental data from Draper Lab are shown in Chapter 4. The 'B-scan map', 'the target localization', the 'excess path length due to multipath' and their explanation are also detailed in that chapter.

Chapter 2

Deconvolution of Medium Response

2.1 Introduction

This section is devoted to the deconvolution method of signal processing, which extracts information from the received signal on travel time delays, propagation and back-scattering characteristics to improve the resolution of medium impulse response. Due to the multiple reflections and refractions of the water column, the received signal is generally mix-phased. Therefore, the conventional linear Wiener filtering, which assumes the minimum phase property, is useless. In order to solve this problem, two steps are taken. First, a homomorphic filter (complex cepstrum) is applied to separate the minimum phase part and maximum phase part, and deconvolve the wavelet for both parts. Then, the medium impulse response is deconvolved by means of Wiener filter with the deconvolved wavelet as the transmitted signal.

2.2 Homomorphic system

The problem of filtering signals, which have been combined by convolution, is very common in underwater signal processing. It would be advantageous to change convolution to addition by applying the appropriate filtering. This leads to a new class of systems called *homomorphic systems* which obey the *generalized principle of superposition.*

Let $'\Diamond'$ be a rule to combine inputs with each other (e.g., addition, multiplication, convolution, etc.) and let $';'$ be a rule to combine inputs with a scalar. Similarly, let $'o'$ denotes a rule to combine outputs and let $'\bullet'$ denote a rule to combine a scalar with an output. Then, the 'homomorphic system' satisfies the following two equations[6],

$$H\{x_1(t) \Diamond x_2(t)\} = H\{x_1(t)\} o H\{x_2(t)\}, \tag{2.1}$$

$$H\{c;x_1(t)\} = c \bullet H\{x_1(t)\}, \tag{2.2}$$

which can be represented by algebraically linear (homomorphic) mappings between input and output signal spaces. Clearly, linear systems are a special case for which '$\Diamond$' and 'o' are addition, and ';' and '$\bullet$' are multiplication. Any homomorphic system can be decomposed as a cascade of three homomorphic systems, as indicated in Fig. 2.1.

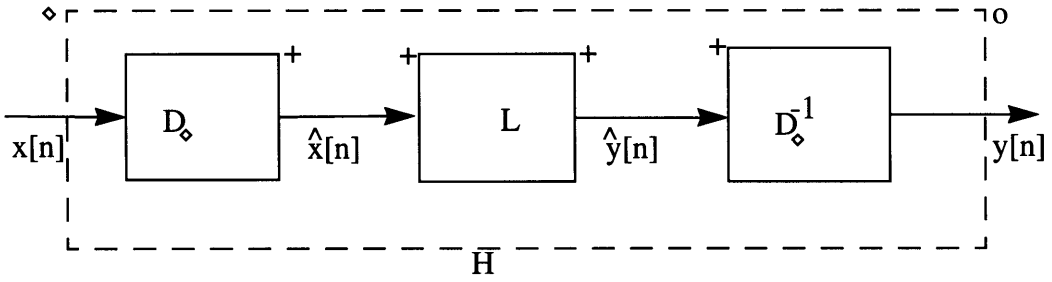

Figure 2.1: Canonical representation of homomorphic systems

Where H means homomorphics system, '$\Diamond$' is a rule to combine inputs and 'o' is a rule to combine outputs.

System D has the following properties:

$$D\{x_1(t) \Diamond x_2(t)\} = D\{x_1(t)\} + D\{x_2(t)\} = \hat{x}_1(t) + \hat{x}_2(t), \tag{2.3}$$

$$D\{c;x_1(t)\} = c \bullet D\{x_1(t)\} = c\hat{x}_1(t). \tag{2.4}$$

The effect of the system D is to transform the signals $x_1(t)$ and $x_2(t)$ according to the rule '$\Diamond$' into a conventional linear combination of corresponding signals $D\{x_1(t)\}$ and $D\{x_2(t)\}$. The system L is a linear system:

$$L\{\hat{x}_1(t) + \hat{x}_2(t)\} = L\{x_1(t)\} + L\{x_2(t)\} = \hat{y}_1(t) + \hat{y}_2(t), \tag{2.5}$$

$$L\{c\hat{x}_1(t)\} = cL\{\hat{x}_1(t)\} = c\hat{y}_1(t). \tag{2.6}$$

System D^{-1} is the inverse of system D, it transforms from addition to the rule 'o':

$$D^{-1}\{\hat{y}_1(t)+\hat{y}_2(t)\} = D^{-1}\{\hat{y}_1(t)\} o D^{-1}\{\hat{y}_2(t)\} = y_1(t) o y_2(t)\,, \tag{2.7}$$

$$D^{-1}\{c\hat{y}_1(t)\} = c \bullet D^{-1}\{\hat{y}_1(t)\} = c \bullet y_1(t)\,. \tag{2.8}$$

The use of a system of the form of Figure 2.1 to remove or alter one of the components of a convolution is called *homomorphic deconvolution.* To understand how this class of homomorphic systems might be useful for deconvolution, consider a signal that is the convolution of two components, i.e.,

$$x(t) = x_1(t) \otimes x_2(t)\,, \tag{2.9}$$

where $'\otimes'$ is the convolution operator $x(t) = \int x_1(\tau)\, x_2(t-\tau)\, d\tau$. For example, $x_2(t)$ might be the impulse response of a stable linear time-invariant system, the effects of which we are interested in, i.e., we would like to recover $x_2(t)$ from $x(t)$. According to Eq. 2.3

$$\hat{x}(t) = \hat{x}_1(t) + \hat{x}_2(t)\,. \tag{2.10}$$

Now, if we can find a choice for the linear system L in Figure 2.1 such that its output is

$$\hat{y}(t) = \hat{x}_2(t)\,, \tag{2.11}$$

then the corresponding output of the overall system in Figure 2.1 will be

$$y(t) = x_2(t)\,. \tag{2.12}$$

In other words, if the linear system removes $x_1(t)$ completely from the additive combination of Eq. 2.10, then $x_1(t)$ is removed from the convolutional combination of Eq. 2.9. In the next section, system D is chosen as the complex cepstrum.

2.3 Complex Cepstrum

Definition and Realization of Complex Cepstrum

The *complex cepstrum*[7], $\hat{x}(t)$, is defined as the inverse Fourier transform of the complex logarithm of the Fourier transform of a signal,

$$\hat{x}(t) = F^{-1}[\hat{X}(\omega)] = F^{-1}[\log(X(\omega))], \tag{2.13}$$

where $F^{-1}[X(\omega)] = \frac{1}{2\pi}\int X(\omega)\, e^{i\omega t} d\omega$.

It is know that convolution in the time domain maps into multiplication in the frequency domain:

$$y(t) = x(t) \otimes h(t), \tag{2.14}$$

$$Y(\omega) = X(\omega) H(\omega). \tag{2.15}$$

When the logarithm is taken,

$$\log[Y(\omega)] = \log[X(\omega) H(\omega)] = \log[X(\omega)] + \log[H(\omega)], \tag{2.16}$$

i.e., $\hat{Y}(\omega) = \hat{X}(\omega) + \hat{H}(\omega)$.

Taking the inverse Fourier transform, we get

$$\hat{y}(t) = \hat{x}(t) + \hat{h}(t), \tag{2.17}$$

since the inverse Fourier transform is a linear operation.

It can be seen from above that the complex logarithm plays a key role in the definition of the complex cepstrum. In order that $\hat{X}(\omega)$ be analytic and have the property that if $X(\omega) = X_1(\omega) X_2(\omega)$, then $\hat{X}(\omega) = \hat{X}_1(\omega) + \hat{X}_2(\omega)$, $\hat{X}(\omega)$ must be defined as

$$\hat{X}(\omega) = \log|X(\omega)| + j\arg[X(\omega)], \tag{2.18}$$

where $\arg[X(\omega)] = ARG[X(\omega)] + 2\pi N(\omega)$, $-\pi < ARG[X(\omega)] \le \pi$, and $N(\omega)$ takes on the appropriate integer values to "unwrap" the principle value of the phase resulting in a continuous curve.

With $x(t)$ real, $\arg[X(\omega)]$ can always be specified so that it is an odd periodic function of ω. With $\arg[X(\omega)]$ an odd function of ω and $\log|X(\omega)|$ an even function of ω, the complex cepstrum $\hat{x}(t)$ is guaranteed to be real.

The complex logarithm can also be defined from its derivative[8]. If one assumes a single valued differentiable complex logarithm (principle value) and the analyticity of $X(\omega)$, one can derive the follows:

$$\frac{d\hat{X}(\omega)}{d\omega} = \frac{d}{d\omega}[\log|X(w)| + j\arg(X(\omega))] = \frac{1}{X(\omega)}\frac{dX(\omega)}{d\omega}. \tag{2.19}$$

And since

$$X(\omega) = X_R(\omega) + jX_I(w), \tag{2.20}$$

we obtain

$$\hat{X}_I'(\omega) = \frac{d}{d\omega}[\arg(X(\omega))] = \frac{X_R(\omega)X_I'(\omega) - X_I(\omega)X_R'(\omega)}{X_R^2(\omega) + X_I^2(\omega)}, \tag{2.21}$$

$$\arg[X(\omega)] = \int_0^{\omega} \hat{X}_I'(\theta)\,d\theta. \tag{2.22}$$

Note that the condition $\arg[X(\omega)]_{\omega=0} = 0$ is implicit in Eq. 2.22, thereby ensuring that $\arg[X(\omega)]$ is an odd function of ω. Eq. 2.21 can be computed very fast using the FFT according to

$$X_R'(\omega) + jX_I'(\omega) = -jFFT[nx(n)]. \tag{2.23}$$

This algorithm works well as long as the spectrum does not have any zeros close to the unit circle, otherwise, the derivative given by the previous relationship and computed by FFT has singularities and presents big spikes. To improve the algorithm, an idea has been suggested by Bhanu[9]. It consists of fitting a curve to the phase derivatives before performing the numerical integration. Suppose the cubic spline $S(\omega)$ which has continuous first and second derivatives is fitted to the phase derivative. The phase is then given by

$$\arg X(\omega) = \int_0^{\omega} S(\omega)\, d\omega, \tag{2.24}$$

or, according to [10]

$$\arg [X(\omega_{i+1})/\omega_i] = \arg X(\omega_i) + \frac{1}{2}\Delta\omega\left[\frac{d}{d\omega}\arg X(\omega_{i+1}) + \frac{d}{d\omega}\arg X(\omega_i)\right]$$

$$-\frac{1}{12}\Delta\omega^2\left[\frac{d}{d\omega}S(\omega_{i+1}) - \frac{d}{d\omega}S(\omega_i)\right], \tag{2.25}$$

where $\frac{d}{d\omega}S(\omega) = \frac{d^2}{d^2\omega}\arg X(\omega)$. This can also be computed by FFT as

$$\frac{d^2}{d^2\omega}\arg X(\omega) = \frac{1}{|X(\omega)|^4}\{|X(\omega)|^2 [X_R(\omega) X_I''(\omega) - X_I(\omega) X_R''(\omega)]$$

$$-2X_R(\omega) X_I(\omega) [(X_R'(\omega))^2 - (X_I'(\omega))^2]$$

$$+ 2X_R'(\omega) X_I'(\omega) [X_I^2(\omega) - X_R^2(\omega)]\}, \tag{2.26}$$

and

$$X_R''(\omega) + jX_I''(\omega) = -FFT[n^2 x(n)]. \tag{2.27}$$

Properties of the complex cepstrum

The complex cepstrum has some properties which are useful for the design of filters and transmitted signals[6]. Some of these properties are summarized below.

1. The complex cepstrum of a convolution of two or more signals is the sum of individual complex cepstrum.

2. The complex cepstrum $\hat{x}(n)$ of a minimum phase sequence $x(n)$ is zero for $n \le 0$,and the complex cepstrum of a maximum phase sequence is zero for $n \ge 0$. (See Appendix A).

3. The complex cepstrum of a pulse whose spectrum is smooth tends to be concentrated around low qufrency values.

4. The complex cepstrum of a periodic impulse train is a periodic impulse train with the same period.

Sensitivity of the complex cepstrum to noise

Since the complex cepstrum is a non-linear system, addition in the time domain does not map to a convenient function in the cepstral domain. Therefore, additive noise makes the phase unwrapping a difficult task. In real life, the signal can usually be expressed as:

$$S(t) = y(t) + n(t), \tag{2.28}$$

where $y(t)$ is the convolution of two or more signals and $n(t)$ is the additive noise. In the frequency domain this equation becomes

$$\log S(\omega) = \log\left(Y(\omega) + N(\omega)\right) = \log\left(Y(\omega)\left(1 + \frac{N(\omega)}{Y(\omega)}\right)\right), \tag{2.29}$$

i.e.,

$$\log|S(\omega)| = \log|Y(\omega) + N(\omega)| = \log|Y(\omega)| + \log\left|1 + \frac{N(\omega)}{Y(\omega)}\right|, \tag{2.30}$$

$$\arg S(\omega) = \arg\left(Y(\omega) + N(\omega)\right) = \arg Y(\omega) + \arg\left(1 + \frac{N(\omega)}{Y(\omega)}\right). \tag{2.31}$$

Even when the signal-to-noise ratio is greater than 1, it is still difficult to say that $\arg Y(\omega)$ is greater than $\arg\left(1 + \frac{N(\omega)}{Y(\omega)}\right)$, although $\log|Y(\omega)|$ dominates in $\log|S(\omega)|$. In that case, Eq. 2.31 can be approximated as

$$\log S(\omega) = \Phi_S(\omega) = \Phi_Y(\omega) + \operatorname{atan}\left(\frac{\left|\frac{N(\omega)}{Y(\omega)}\right|\sin\left(\Phi_N(\omega) - \Phi_Y(\omega)\right)}{1 + \left|\frac{N(\omega)}{Y(\omega)}\right|\cos\left(\Phi_N(\omega) - \Phi_Y(\omega)\right)}\right), \tag{2.32}$$

where $\Phi_N(\omega)$ and $\Phi_Y(\omega)$ are respectively the phase of noise and the signal. With $\left|\frac{N(\omega)}{Y(\omega)}\right| \ll 1$, Eq. 2.32 becomes $\Phi_S(\omega) \approx \Phi_Y(\omega)$.

Eq.2.31 shows that the phase of the received signal $s(t)$ will become unpredictable (random) because of the additive noise. However, if the ambient noise is standard white

noise, it works as a DC component in the spectral domain that maps only to the point t=0 of cepstrum domain. The part of the noise spectrum which is not overlapped by the signal spectrum can be removed by band-pass filtering in order to avoid the situation of a low signal-to-noise ratio.

The use of band-pass mapping before the homomorphic deconvolution leads to the notion of band-pass mapping systems which will be discusses in section 2.5.

2.4 Wiener filter

The goal of this section is to provide a method to deconvolve the medium impulse response, which contains much information about the underwater targets. Since the homomorphic deconvolution was not the best for estimating the medium response with the presence of additive noise, a digital Wiener (Optimal) filter will be used. It belongs to the class of linear time-invariant filters with a criterion of minimization of the least square error[11].

As expressed before, the received signal has the following form:

$$s(k) = r(k) \otimes w(k) + n(k) = y(k) + n(k) , \tag{2.33}$$

where $w(k)$ and $r(k)$ are, respectively, the wavelet and the medium impulse response deconvolved by the complex cepstrum. In the absence of noise, the effects of the medium response $r(k)$ are deconvolved through dividing $Y(z)$ by $W(z)$, i.e.,

$$R(z) = \frac{Y(z)}{W(z)} , \tag{2.34}$$

where $Y(z), W(z)$, and $R(z)$ are the z-transforms of $y(k), w(k)$, and $r(k)$ respectively. Now, it is necessary to find the optimal filter $h(k)$ or $H(z)$, which, when applied to the measured signal $s(k)$ or $S(z)$, produces a medium response $\hat{r}(k)$ or $\hat{R}(z)$ that is as close as possible to the real medium response. In other words, the true medium response can be estimated by

$$\hat{R}(z) = S(z) H(z) . \tag{2.35}$$

In order to make $\hat{R}(z)$ be close to $R(z)$, it is required that they be close in the least square sense, i.e.,

$$\sum_{k=-\infty}^{\infty} |\hat{r}(k) - r(k)|^2 = \int_{-\infty}^{\infty} |\hat{R}(z) - R(z)|^2 dz , \tag{2.36}$$

is minimized.

Substituting Eq. 2.33--2.35 into Eq. 2.36 and because the signal and the noise are uncorrelated, their cross product, when integrated over z, gives zero. Eq. 2.36 will be a minimum if and only if the integrand is minimized with respect to $H(z)$ at every value of z. Differentiating with respect to $H(z)$, and setting the result equal to zero gives

$$H(z)\,[|Y(z)|^2 + |N(z)|^2] = \frac{|Y(z)|^2}{W(z)}. \tag{2.37}$$

This is the formula for Wiener filter (optimal) $H(z)$.

To determine the Wiener filter from Eq. 2.37 we need some other ways of separately estimating $|Y|^2$ and $|N|^2$. There is no way to do this from the measured signal S alone without some other information, assumption or guess. Eq. 2.37 tells us that H looks like the quotient of the model of signal power to the model of signal plus noise power weighted by wavelet. Notice that H will be close to $1/W$ where the noise is negligible, and close to zero where the noise is dominant. That is how it does its job! The intermediate dependence given by Eq. 2.37 just turns out to be the optimal way of going in between these two extremes.

Computational Realization of Wiener Filter

Let C_{yy} be the autocorrelation of sequence $y(k)$ (zero mean), then the spectral density $\Gamma_{yy}(z)$ $(|z| = 1)$ of this sequence is

$$\Gamma_{yy}(z) = \sum_{m=-\infty}^{\infty} C_{yy}(m)\,z^{-m} = \sum_{m=-\infty}^{\infty}\sum_{k=-\infty}^{\infty} y(k)\,y(k+m)\,z^{-m} = Y^*(z)\,Y(z) = |Y(z)|^2. \tag{2.38}$$

Similarly,

$$\Gamma_{nn}(z) = |N(z)|^2, \Gamma_{ww}(z) = |W(z)|^2. \tag{2.39}$$

Suppose both the medium response $r(k)$ and noise $n(k)$ are uncorrelated sequences,

i.e.,

$$E[r(k)\,r(k+m)] = \sum_{k=-\infty}^{\infty} r(k)\,r(k+m) = 0, \quad \text{with } m \neq 0, \tag{2.40}$$

then,

$$\Gamma_{rr}(z) = \sum_{m=-\infty}^{\infty}\sum_{k=-\infty}^{\infty} r(k)\,r(k+m)\,z^{-m} = \sum_{k=-\infty}^{\infty} r(k)\,r(k) = R_{rr}(0), \tag{2.41}$$

$$\Gamma_{yy}(z) = \Gamma_{rr}(z)\,\Gamma_{ww}(z) = R_{rr}(0)\,\Gamma_{ww}(z), \Gamma_{nn}(z) = R_{nn}(0). \tag{2.42}$$

Substituting Eq. 2.38-2.39, and Eq. 2.41-2.42 into Eq. 2.37 yields

$$H(z)\left[\Gamma_{ww}(z) + \frac{R_{nn}(0)}{R_{rr}(0)}\right] = W^*(z). \tag{2.43}$$

Coming back into the time domain, for the minimum phase condition, Eq. 2.43 assumes the form

$$\sum_{k=0}^{p-1} h(k)\left[C_{ww}(m-k) + \frac{R_{nn}(0)}{R_{rr}(0)}\delta(m-k)\right] = w(-m), \ (m \in [0, p-1]). \tag{2.44}$$

For maximum phase condition, Eq. 2.43 assumes:

$$\sum_{k=0}^{-p+1} h(k)\left[C_{ww}(k-m) + \frac{R_{nn}(0)}{R_{rr}(0)}\delta(k-m)\right] = w(-m), \ (m \in [-p+1, 0]), \tag{2.45}$$

where C_{ww}, C_{nn}, C_{rr} are respectively the autocorrelation of sequences $w(k), n(k), r(k)$.

In vector space, Eq. 2.44 and Eq. 2.45 can be written as:

$$\left(R_{ww} + \frac{R_{nn}(0)}{R_{rr}(0)}I\right)H = W, \tag{2.46}$$

where

$$H = \begin{bmatrix} h(0) \\ \circ \\ \circ \\ h(p-1) \end{bmatrix}, W = \begin{bmatrix} w(0) \\ \circ \\ \circ \\ w(-p+1) \end{bmatrix}, R_{ww} = \begin{bmatrix} C_{ww}(0) & C_{ww}(-1) & \circ & C_{ww}(-p+1) \\ \circ & C_{ww}(0) & \circ & \circ \\ \circ & \circ & \circ & \circ \\ C_{ww}(p-1) & \circ & \circ & C_{ww}(0) \end{bmatrix}. \quad (2.47)$$

Now it is necessary to estimate R_{ww} through $w(k)$ (the wavelet deconvolved by the complex cepstrum) and R_{nn}/R_{rr} through the following steps (see Appendix A).

(1) Compute the eigenvalues σ_i of the correlation matrix R_{ss}, i.e., $R_{ss} = R_{yy} + R_{nn}(0)I$.

(2) Compute the eigenvalues α_i of the correlation matrix R_{ww}.

(3) Estimate the rank Q of the correlation matrix R_{ww} by finding q=Q at which the function $f(q)$ arrives its minimum:

$$f(q) = (P-q)\ln\left(\frac{1}{P-q}\sum_{i=q+1}^{P}\sigma_i\right) - \sum_{i=q+1}^{P}\ln(\sigma_i) + q(P+0.5-q/2). \quad (2.48)$$

(4) Estimate $R_{nn}(0)$ by taking the average of the P-Q smallest eigenvalues σ_i (the eigenvalues are arranged in decreasing order):

$$R_{nn}(0) = \frac{1}{(P-Q)}\sum_{i=Q+1}^{P}\sigma_i. \quad (2.49)$$

(5) Estimate the eigenvalues λ_i of R_{yy} from $\lambda_i = \sigma_i - R_{nn}(0)$.

(6) Estimate $R_{rr}(0)$ by means of $R_{rr}(0) = Q^{-1}\sum_{i=1}^{Q}\frac{\lambda_i}{\alpha_i}$.

(7) Compute $R_{nn}(0)/R_{rr}(0)$.

2.5 Combination of homomorphic deconvolution and Wiener Filtering

Although the Wiener filter is well defined for a minimum or maximum phase input sequence, it is rather unstable for a mixed phase sequence. Since the received signal and wavelet are mixed phase in real life, an idea is to factorize the received signal and wavelet into their minimum and maximum phase components. Then in order to improve the deconvolution method, we can apply a zero-lag causal Wiener and anti-causal Wiener filter to the minimum and maximum phase component, respectively.

Definition and implementation of the band-pass mapping system

In general the signals are band-pass filtered before being sampled in order to increase the signal-to-noise ratio. The complex cepstrum cannot be applied directly to the band-pass signal, since the logarithm is not defined in the frequency domain where the signal vanishes. Before applying any cepstrum analysis, it is necessary to transform the band-pass signal into a full band signal. Such a system is called a band-pass mapping system[7].

The band-pass signal satisfies

$$X(\omega) \neq 0,\ \omega_1 \leq |\omega| \leq \omega_2 \text{ otherwise } X(\omega) = 0, \tag{2.50}$$

where ω_1 and ω_2 are the cut off frequencies. Let $\tilde{X}(\tilde{\omega})$ denote the signal after band-pass mapping system, then

$$\tilde{X}(\tilde{\omega}) = X(\omega),\ 0 \leq |\tilde{\omega}| \leq \pi, \tag{2.51}$$

where $\tilde{\omega}(\omega) = \dfrac{\omega - \omega_1}{\omega_2 - \omega_1},\ \omega_1 \leq |\omega| \leq \omega_2$.

Tribolet[8] has verified that the band-pass mapping is an invertible homomorphic operation. Let $x(n)$ be N samples sequence and $X(k)$ the corresponding DFT sequence. The center frequency corresponds to the frequency sample $\frac{N}{4}$ (i.e., normalized frequency 0.5); the cut-off frequencies correspond to $\frac{N}{4} - N_1$ and $\frac{N}{4} + N_1$. The operation of band-pass mapping can be decomposed into the following steps.

1. Shift the band-pass spectrum to 0.

2. Compute the $2N_1 + 1$ IDFT of the sequence X(k) for $\frac{1}{4}N - N_1 < k < \frac{1}{4}N + N_1$.

3. Zero-pad the new time series to get a time sequence of N samples.

The inverse band-pass mapping operation can be broken down into the following phases.

1. Cut the N samples of the deconvolved sequence at the first $2N_1 + 1$ samples.

2. Compute the DFT of $2N_1 + 1$ sequence.

3. Shift the spectrum to the $\frac{N}{4} - N_1$ frequency sample; set the spectrum value $X(k)$ at 0 for $1 < k < \frac{1}{4}N - N_1 - 1$ and $\frac{1}{4} + N_1 + 1 < k < \frac{1}{4}N$.

4. Compute the N IDFT.

Normalization of the signal before applying the cepstrum

When the time series $\tilde{x}(n)$ (after band-pass mapping) does not fulfill the requirements that its DC component (polarity) is positive and its mean phase derivative is equal to zero, the input sequence $\tilde{x}(n)$ must be normalized before applying complex cepstrum[6]. The first part of normalization consists of multiplying $\tilde{X}(\omega)$ by $e^{(-j\omega\tau)}$ (τ is the mean phase derivative of $\tilde{x}(n)$. The second part of the normalization consists of multiplying $\tilde{X}(\omega)$ by the polarity. It seems that the linear phase and the polarity is lost after normalization. However, the cepstrum, in this thesis, is applied only to separate the minimum phase part and maximum phase part, which are used to construct the Wiener filter (Figure 2.2), the lost information can be recovered from the convolution of Wiener filter and the received signal. Actually, what Wiener filter does is the removal of noise.

Factorization of the mixed phase signal

The received signal $s(t) = w(t) \otimes r(t) + n(t)$, in the z-domain, is of the form

$$S(z) = W(z)R(z) + N(z) . \tag{2.52}$$

Suppose that the $S(z)$ is a rational transfer function, and $W(z)$ can be factorized as follows:

$$W(z) = W_{minp}(z)\,W_{maxp}(z) , \tag{2.53}$$

where $W_{minp}(z)$ and $W_{maxp}(z)$ are respectively the minimum and maximum pulse components of $W(z)$. Similarly, $R(z)$ can be factorized as follows

$$R(z) = R_{minp}(z)\,R_{maxp}(z) . \tag{2.54}$$

Therefore, $S(z)$ can be rewritten in the form of:

$$S(z) = [W_{minp}(z)R_{minp}(z)]\,[W_{maxp}(z)R_{maxp}(z)] + N(z)$$

$$= S_{minp}(z)\,S_{maxp}(z) , \tag{2.55}$$

where $S_{minp}(z) = W_{minp}(z)R_{minp}(z) + N_1(z)$, and $S_{maxp}(z) = W_{maxp}(z)R_{maxp}(z) + N_2(z)$.

In the cepstrum domain, the previous Eq. 2.55 becomes

$$\hat{s}(t) = \hat{s}_{minp}(t) + \hat{s}_{maxp}(t) . \tag{2.56}$$

Then by applying the complex cepstrum, we are able to factorized $\hat{s}(t)$ and $\hat{w}(t)$ into their minimum and maximum phase condition because minium phase signal is zero for the negative qufrency and maximum phase signals equal zero for the positive qufrency.

Procedure for deconvolving the wavelet and the medium impulse response

To deconvolve the wavelet and estimate the medium impulse response, the following steps are involved.

1. Band-pass mapping of received signal $s(t)$ to get $\tilde{s}(t)$, then normalize $\tilde{s}(t)$.

2. Apply the complex cepstrum to the signal $\tilde{s}(t)$.

3. Filter the complex cepstrum by means of two rectangular windows. The first win-

dow is defined for the positive qufrencies in order to extract the cepstrum $\hat{s}_{minp}(t)$, the second window is defined for the negative qufrencies in order to extract $\hat{s}_{maxp}(t)$.

4. Low-pass filter $\hat{s}_{minp}(t)$ to get $\hat{w}_{minp}(t)$ and high-pass filter $\hat{s}_{maxp}(t)$ to get $\hat{w}_{maxp}(t)$.

5. Design $\tilde{h}_{minp}(t)$ with $\tilde{s}_{minp}(t)$ and $\tilde{w}_{minp}(t)$, and design $\tilde{h}_{maxp}(t)$ with $\tilde{s}_{maxp}(t)$ and $\tilde{w}_{maxp}(t)$.

6. The medium impulse response $\tilde{r}(t)$ is estimated as follows:

$$\tilde{r}(t) = \tilde{s}(t) \otimes \tilde{h}(t) = \tilde{s}(t) \otimes [\tilde{h}_{maxp}(t) \otimes \tilde{h}_{minp}(t)] . \tag{2.57}$$

7. Inverse band-pass mapping of $\tilde{r}(t)$ to get $r(t)$.

The box diagram of this procedure is shown in Figure 2.2,

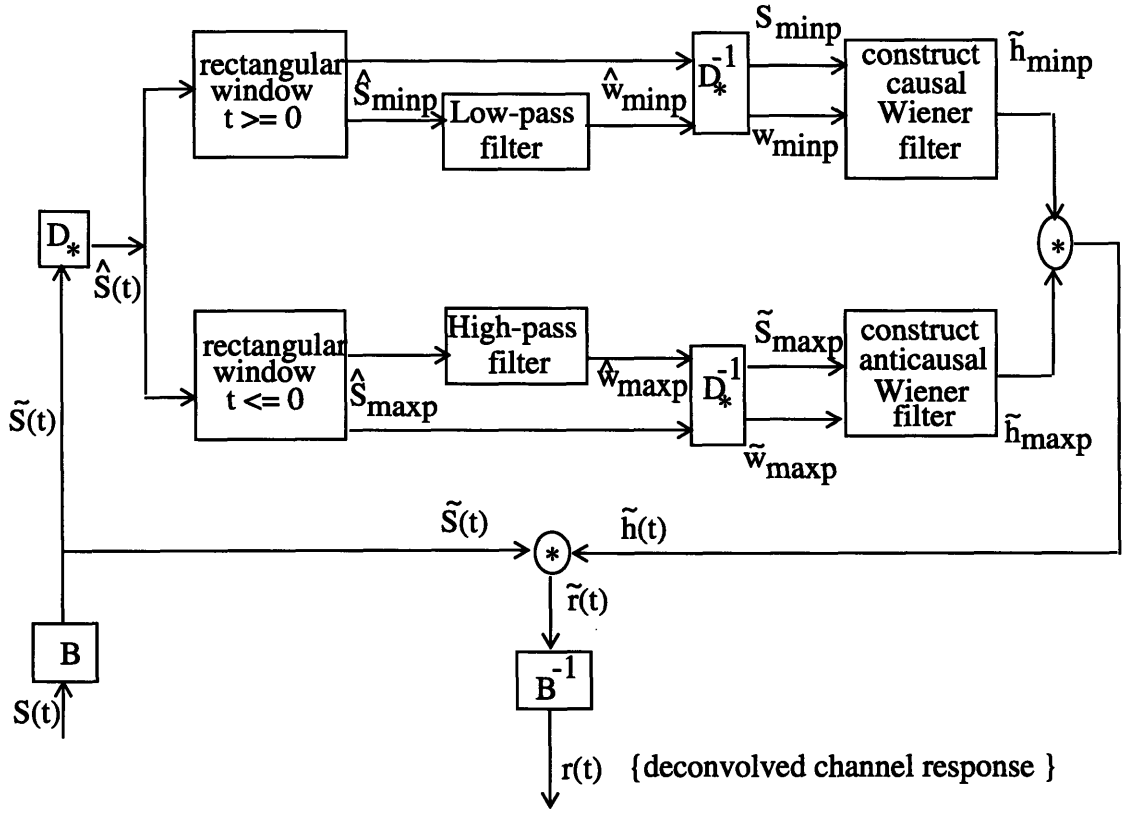

Figure 2.2: Deconvolution procedure

where system B is the band-pass mapping, and B^{-1} is the inverse of system B, and * is the convolution operator.

Chapter 3

Theoretical simulation results

3.1 One-way simulation results

The scenario depicted in Figure 3.1 relates to active sonar propagation. The transmitted signal is windowed CW pulses and the reverberated signal is received on a horizontal towed array. The results prove the feasibility of the methods detailed in chapter 2.

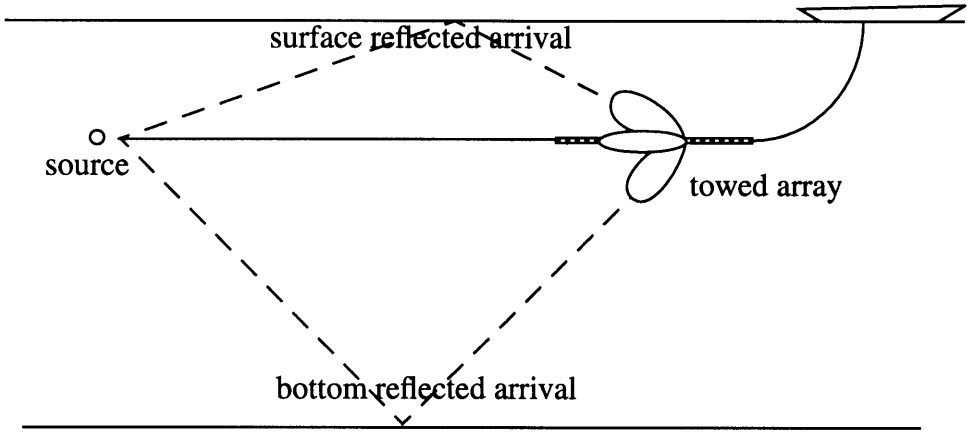

Figure 3.1: Configuration of the active sonar one way transmission

Transmitted signal

The transmitted signal is a Hanning-windowed CW pulse. The pulse length is taken as a parameter of the simulation. The sampled CW pulse is modeled as

$$x(t) = \sin[2\pi f_0 (n-1)]\left[1 - \cos\left(2\pi \frac{(n-1)}{L}\right)\right], \tag{3.1}$$

where L is the pulse length in samples and f_0 is the normalized frequency of the CW signal (i.e., $f_0 = f_c/f_s$, f_c is the center frequency and f_s is the sample frequency). The CW pulse is represented in Fig. 3.3(a), where L is 64 and f_0 equals 0.25.

Medium impulse response

Usually, the reverberation model has one direct path and many multipaths which are

the combination of the surface reflection and bottom reflection or refraction. In this section, we do not model the transfer function of the surface, nor the bottom transfer function. The channel impulse is given by:

$$r(n) = A_1\delta(n-k_1) - A_2\delta(n-k_2) + A_3\delta(n-k_3) - A_4\delta(n-k_4) + \ldots . \tag{3.2}$$

Additive noise

The noise is characterized by its spectrum and the signal-to-noise ratio, and is defined as the response of a linear filter to an input white Gaussian noise (random normal sequence). Since the band-pass mapping system is used before complex cepstrum, the signal-to-noise ratio before and after the band-pass mapping are both important to analyze the simulation and experimental results. The signal-to-noise ratio is calculated in full band as follows:

$$SNR = 10\log\left(\frac{\int_B |Y(f)|^2}{\int_B |N(f)|^2}\right), \tag{3.3}$$

$$BSNR = 10\log\left(\frac{\int_B |\tilde{Y}(f)|^2}{\int_B |\tilde{N}(f)|^2}\right), \tag{3.4}$$

where $N(f)$ and $Y(f)$, are respectively the spectrum of the noise $n(t)$ and the received signal without noise $y(t)$, while $\tilde{N}(f)$ and $\tilde{Y}(f)$ are the corresponding spectrum after band-pass mapping. B is the frequency bandwidth. 'SNR' and '$BSNR$' are called the signal-to-noise ratio before and after band-pass mapping, respectively.

Description of the processing

An observation time of 256 time samples is used and the simulated channel response is combined with three impulses corresponded to $A_1 = 0.9, A_2 = -0.9^4, A_3 = 0.9^6, A_{i>3} = 0$ and $k_1 = 80, k_2 = 110, k_3 = 170$ in Eq. 3.2. The received signal is band-pass filtered in with

a rectangular window defined by the lowest normalized frequency f_{min} = 0.222 and f_{max} = 0.277. The band-pass mapping and the complex cepstrum was applied to get the recovered signal. The medium impulse response is deconvolved by Wiener filter.

Results and their interpretation

Figure 3.2--Figure 3.11 are the results of one-way simulation with different signal-to-noise ratios and different realization of random noise. The transmitted signal and the channel response in these figures are the same. It can be seen that the method is robust for signal-to-noise ratio down to lower than -11db for some realization of random noise. However, sometimes, even when the signal-to-noise ratio is not low, the result is not as good as it for other realizations. In order to analyze this phenomenon, two different realization of random noise are used and are drawn in Figure 3.12. Figure 3.2--Figure 3.8 are of random noise[a] with signal-to-noise ratio from 3.98dB to -11.655dB, which demonstrates that the method detailed in Chapter 2 is successful in recovering the transmitted signal and the channel response. Figure 3.9--Figure 3.11 are of random noise[b]. Figure 3.2, Figure 3.5, Figure 3.6, and Figure 3.9 show us the deconvolved channel response and minimum-phase wavelet under different received signals. Figure 3.4 and Figure 3.11 give us some intuition about the complex cepstrum of noise, transmitted signal and channel response, which tell us that the lower part of the complex cepstrum is mainly from noise and transmitted signal. Figure 3.3, Figure 3.7, Figure 3.8, and Figure 3.10 depict the recovered transmitted signal and the correlation function of the recovered signal and the CW pulse, which indicate that the recovered transmitted signal can be rescaled by correlation with the transmitted pulse. It can be seen from all these figures that the band-pass mapping is very helpful in increasing the signal-to-noise ratio, which is required for applying the complex cepstrum. The difference between *SNR* and *BSNR* of these figures is up to 7.6dB. The deconvolved wavelet in Figure 3.2(b), Figure 3.5(b), Figure 3.6(b), and

Figure 3.9(b) is the wavelet after band-pass mapping. When the signal-to-noise ratio decreases to -11.65dB, there seems not so much information in Figure 3.6(b), the channel response of Figure 3.6(c) and the main frequency of transmitted signal of Figure 3.8(b) can still be resolved, though the shape of transmitted signal cannot be well recovered as shown in Figure 3.8(a). This is because the general shape of the transform of Gaussian white noise is a constant function with many local variations and results in a DC component of the spectrum[12]. Therefore, the white noise maps to the point t=0 of cepstrum domain. So, the low qufrency part of complex cepstrum, especially the point t=0, is more sensitive to the white noise. The Wiener filter, with the deconvolved wavelet as input, can successfully separate the three multipaths shown in Figure 3.2(c), Figure 3.5(c), and Figure 3.6(c). In Figure 3.9(c), the result of Wiener filter is not 'optimal' and the absolute amplitude information of channel response is lost as a consequence of the fact that the real ambient noise is not white enough. Thus, a 'white noise' parameter is needed to add to the zero-lag element of the autocorrelation matrix in order to stabilize the computation of the inverse[13]. The ill-conditioned problem arises because the order of the received signal is smaller than the order of the linear system (channel response), so that the estimation of $R_{nn}(0)/R_{rr}(0)$ is not reasonable as shown in Appendix A. Figure 3.12 says that there is little difference of standard deviation(STD) value between two realizations of random noise, and the larger the STD, the wider the noise cepstrum. It can be concluded that the whiteness might effect the Wiener filter resolution. Moreover, Figure 3.9 shows that the linear phase seems sensitive to the realization of random noise so that the time delay in the channel response cannot be deconvolved properly, though the relative positions of the multipaths are still correct after the Wiener filter.

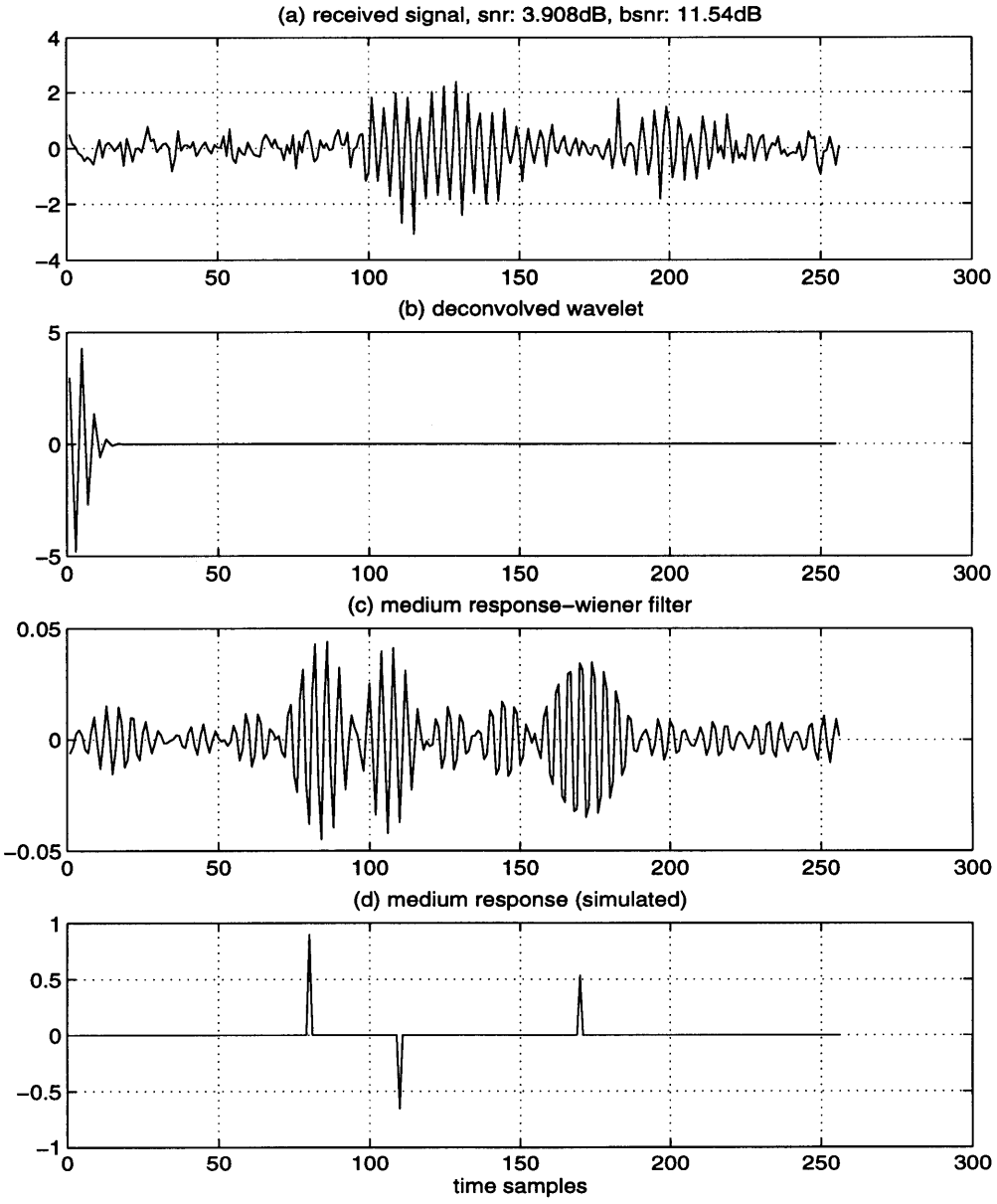

Figure 3.2: Deconvolution of medium response

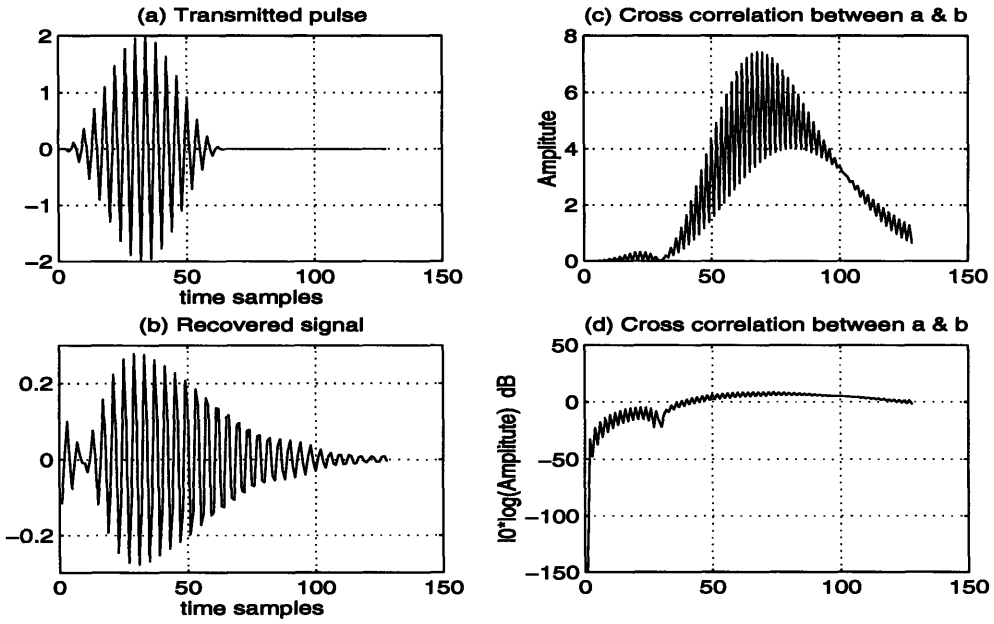

Figure 3.3: Comparison of transmitted signal and recovered signal [correspond to received signal of Figure 3.2(a), snr=3.908dB, bsnr=11.54dB]

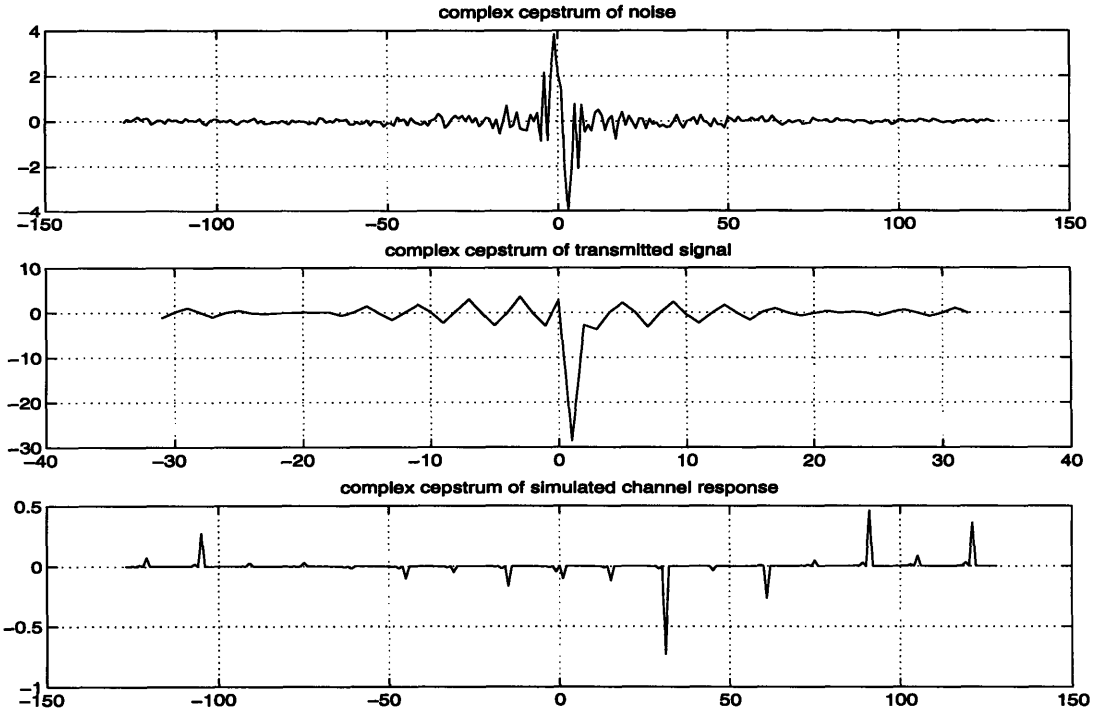

Figure 3.4: Complex cepstrum of noise, CW signal, and simulated channel response [correspond to received signal of Figure 3.2(a), snr=3.908dB,bsnr=11.54dB]

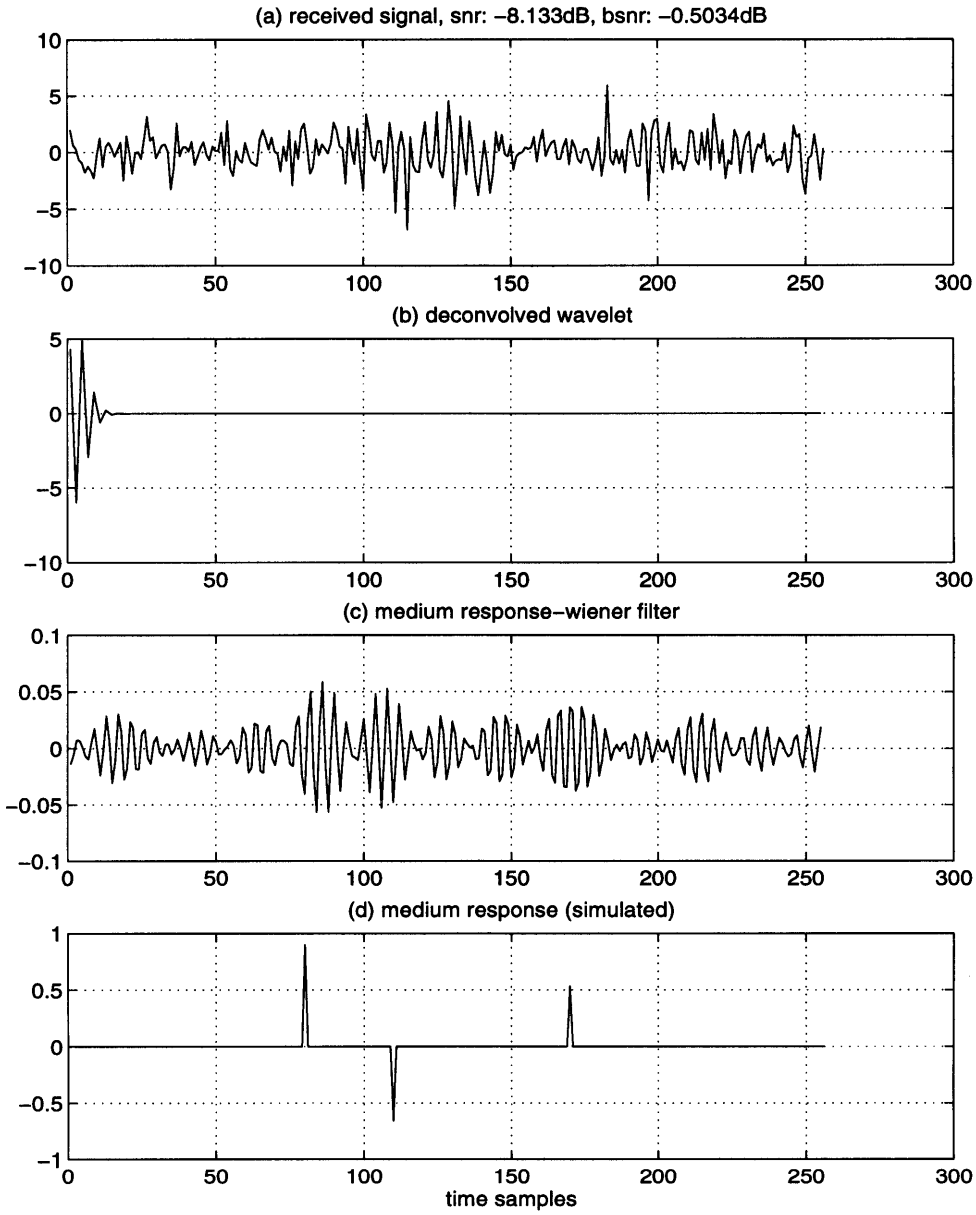

Figure 3.5: Deconvolution of medium response

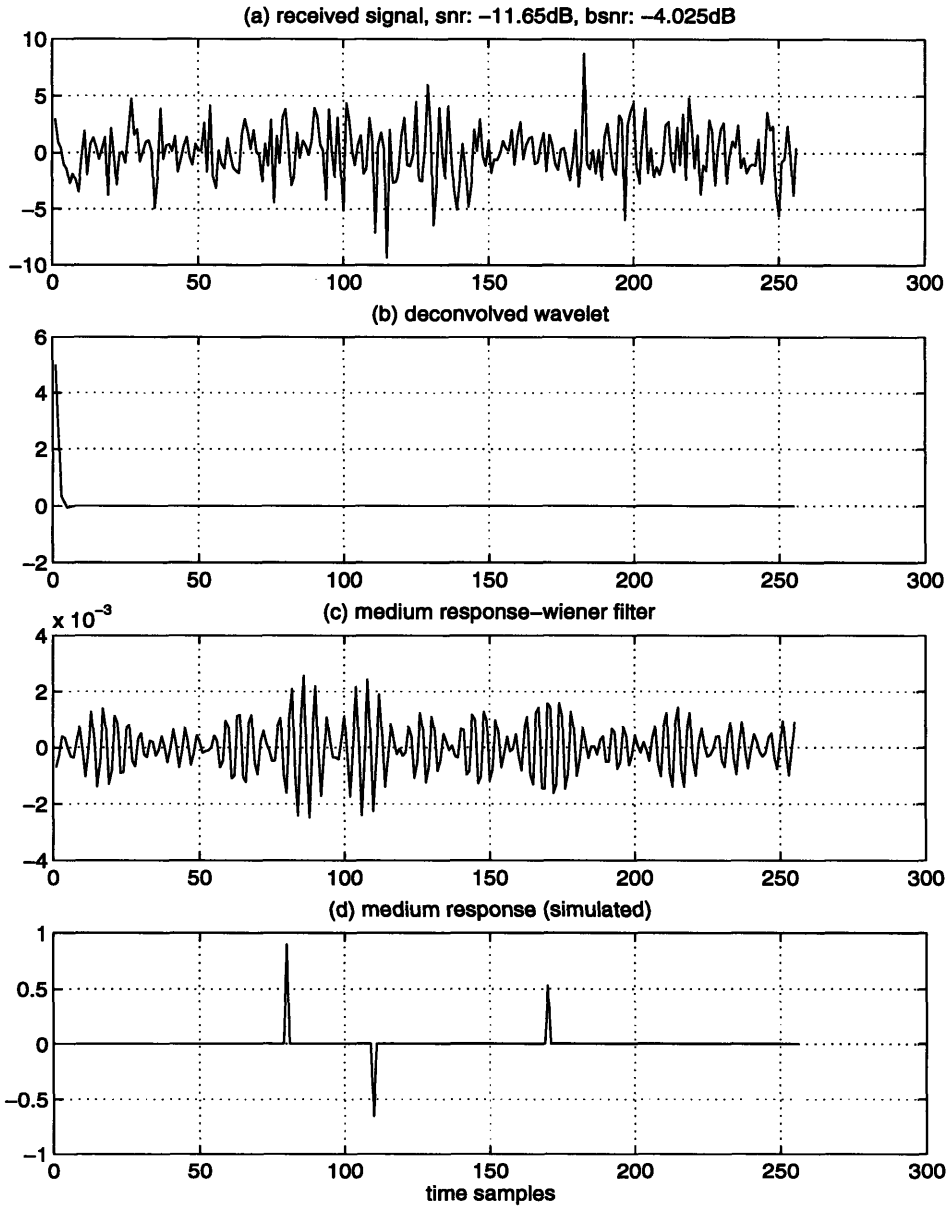

Figure 3.6: Deconvolution of medium response

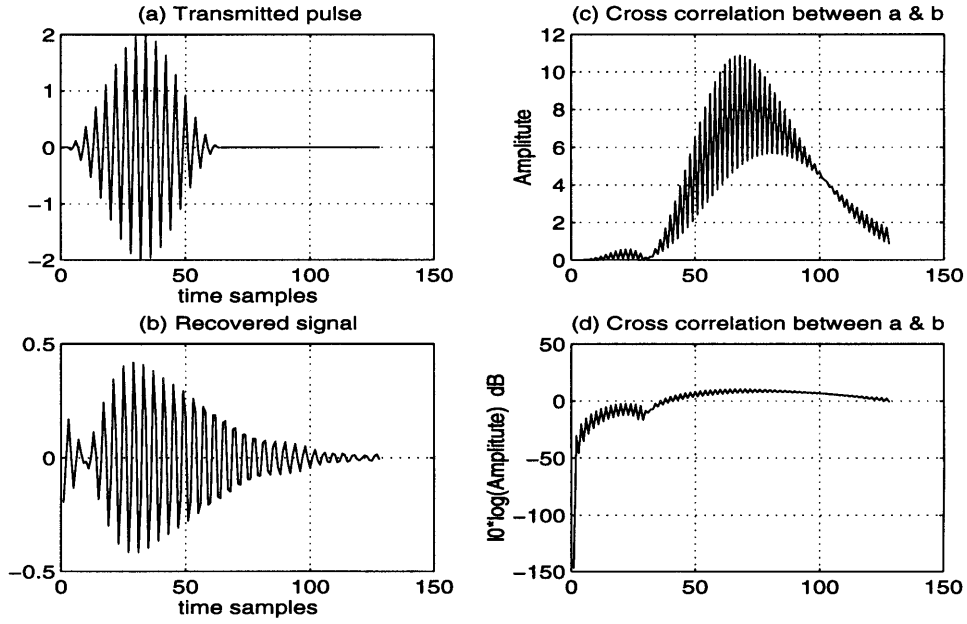

Figure 3.7: Comparison of transmitted signal and recovered signal [correspond to received signal of Fig 3.5(a),snr=-8.133dB, bsnr=0.5034dB]

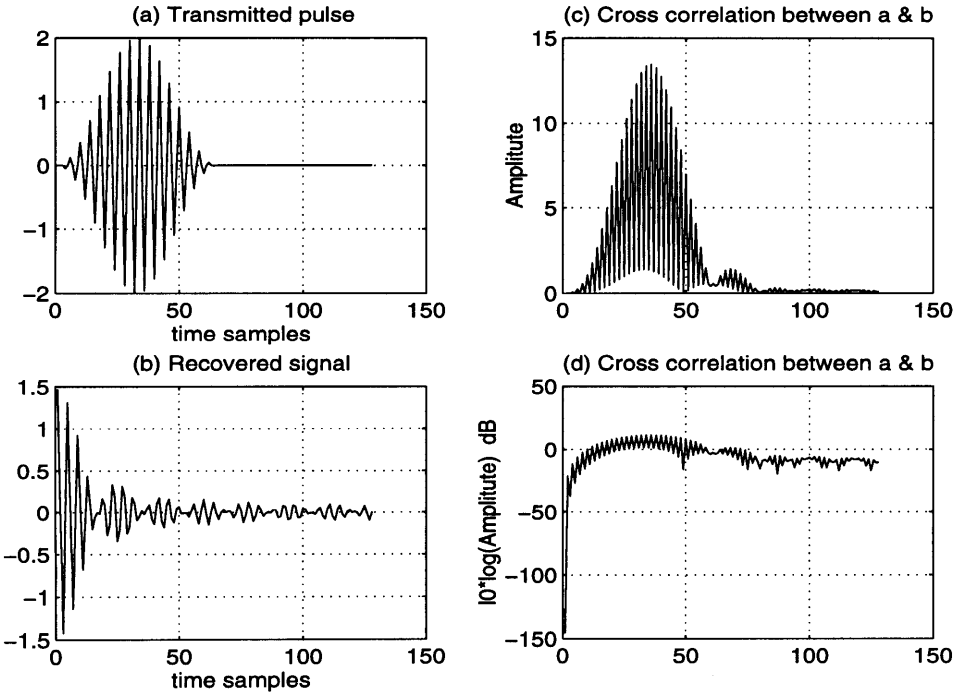

Figure 3.8: Comparison of transmitted signal and recovered signal [correspond to received signal of Fig 3.6(a),snr=-11.65dB, bsnr=-4.025dB]

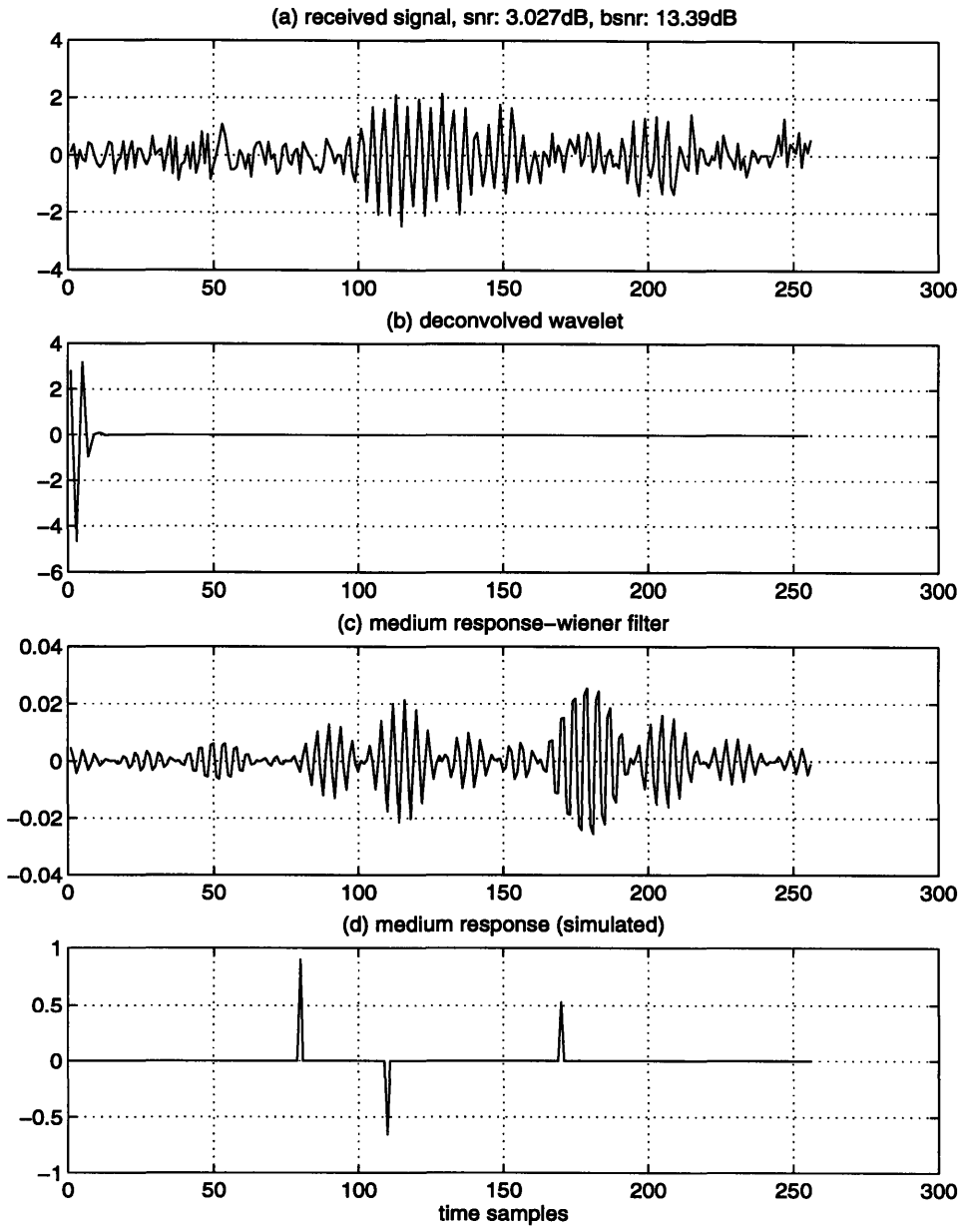

Figure 3.9: Deconvolution of medium response

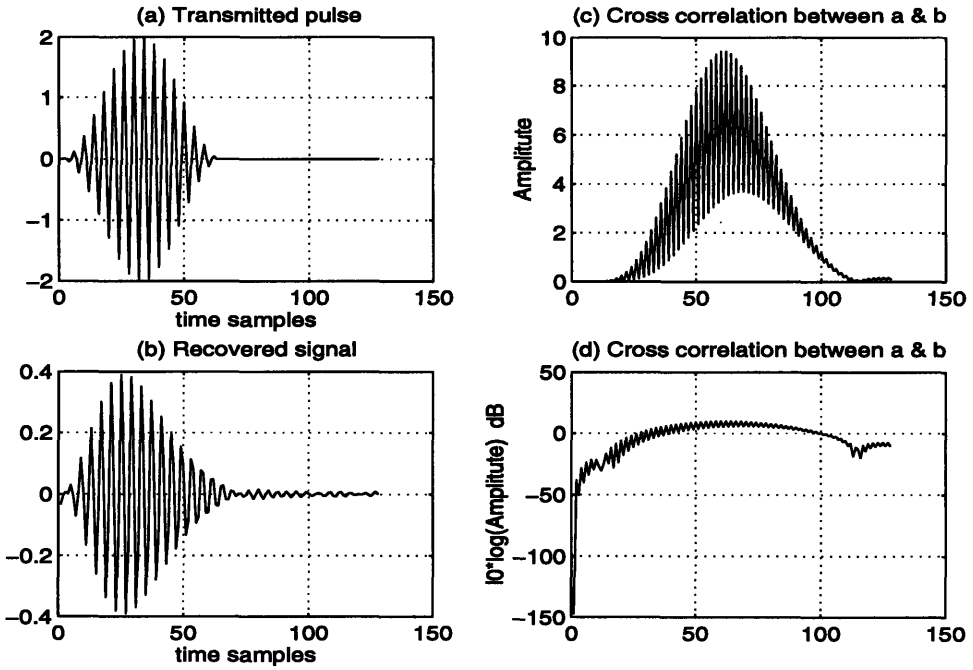

Figure 3.10: Comparison of transmitted signal and recovered signal [correspond to received signal of Fig 3.9(a),snr=3.027dB,bsnr=13.39dB]

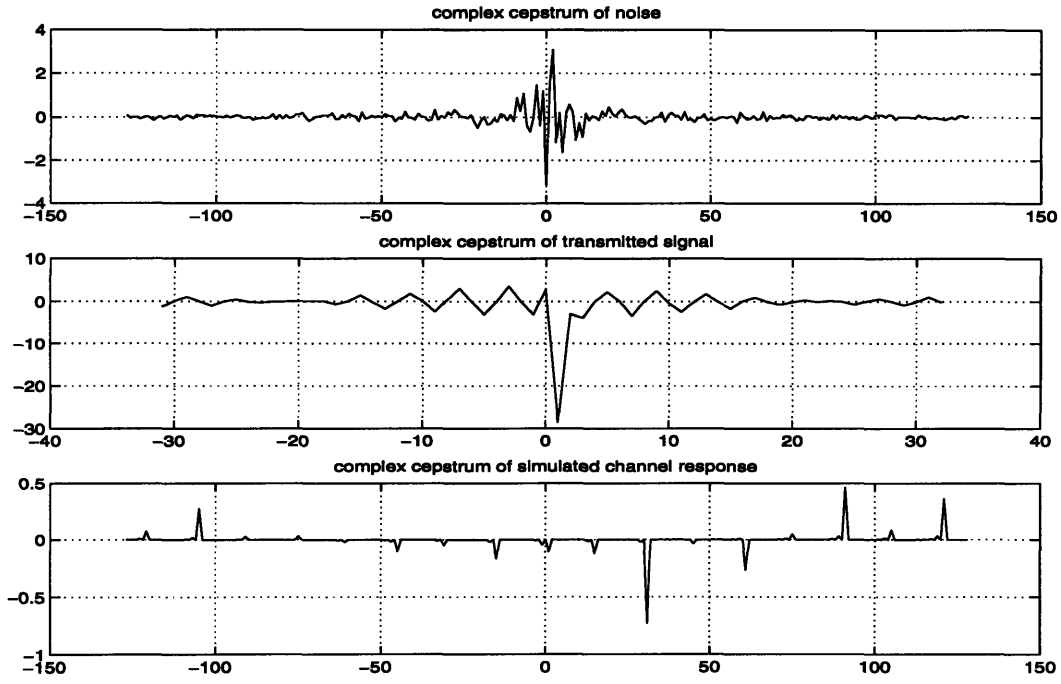

Figure 3.11: Complex cepstrum of noise, CW signal, and simulated channel response [correspond to received signal of Fig 3.9(a),snr=3.027dB,bsnr=13.39dB]

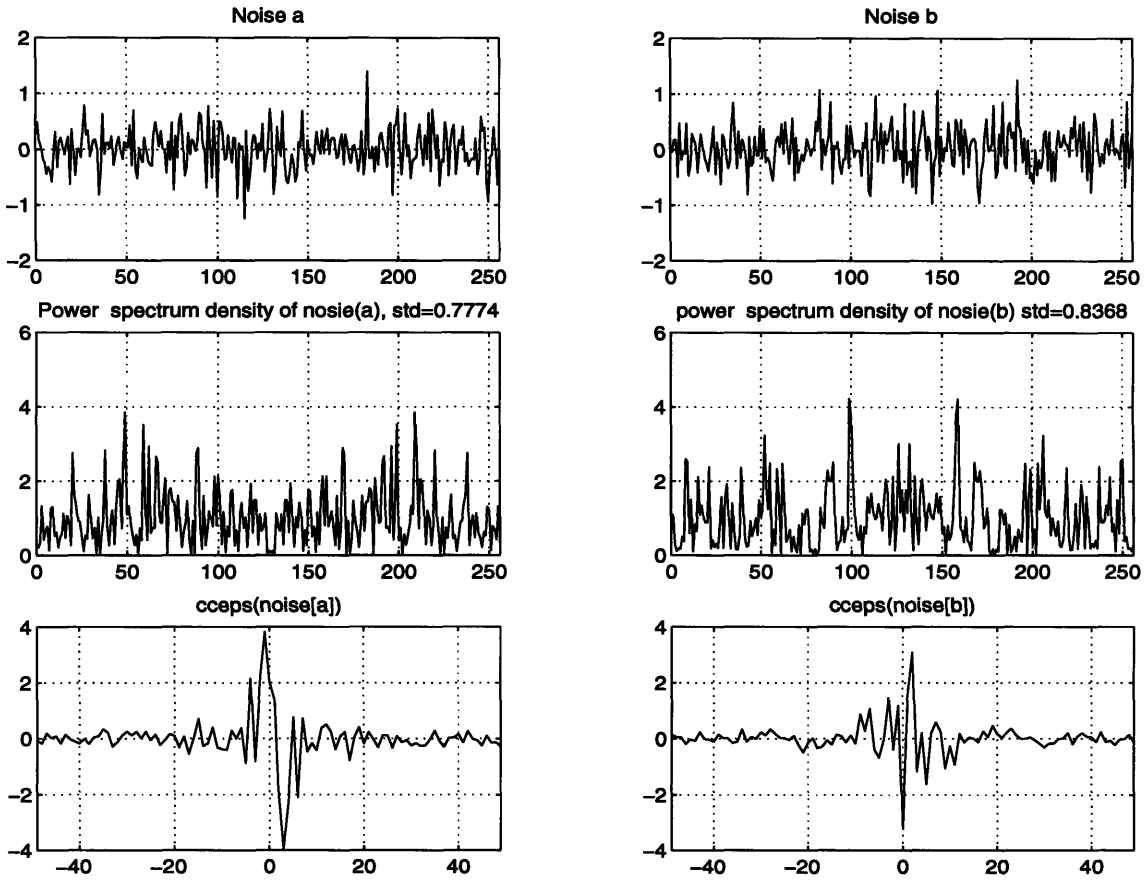

Figure 3.12: Comparison of two realizations of random noise

3.2 Two-way simulation results

The scenario depicted in Figure 3.13 is a typical two-way reverberation in shallow water. The channel is characterized with the following parameters:

D : Channel depth (35m).

Ds: Depth of source and receiver (range from 3 to 32m).

Dt: Depth of target (ranges from 3 to 32m).

L : Range from source to target (200m).

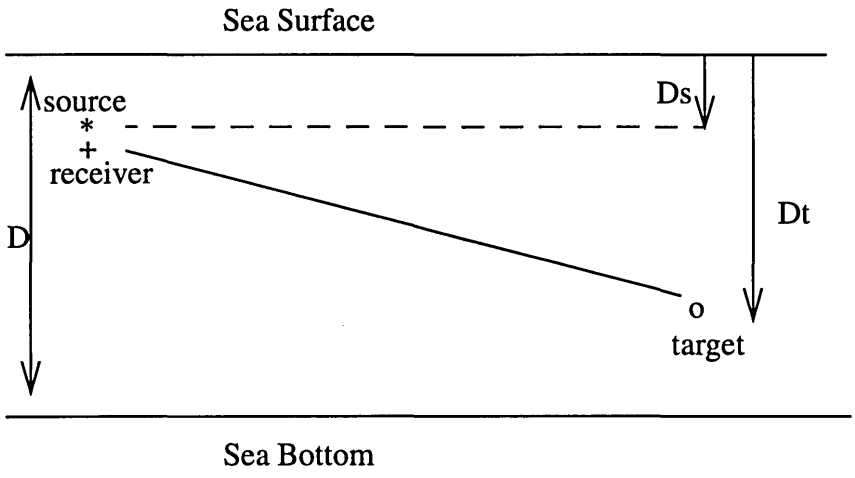

Figure 3.13: Configuration of two way transmission

Description of the signals, impulse response and noise.

The signal used here is a 10 kHz gated sine wave of pulse length 0.33ms with a 3 kHz bandwidth shown in Figure 3.15(a), Figure 3.18(a), and Figure 3.21(a). Since the range from source to target is only 200m, it is reasonable to assume the iso-velocity profile and use ray tracing mode to calculate the two-way channel response shown in Figure 3.14, Figure 3.17, and Figure 3.20. Zero mean random Gaussian noise is added to the convolved signal at different levels of variance. The received signal is the one after the matched filter[14], which cuts out all the noise that is not in the bandwidth of the original signal and

much of the noise in the signal's frequency band that is not correlated with the signal.

Description of the processing

An observation time of 2048 time-samples (about 41ms) has been used and the pulse length is equal to 16 time-samples (about 0.33ms).The received signal is first matched filtered and then band-passed filtered with a rectangular window defined by the bandwidth of the transmitted signal. After that, we apply the band-pass mapping and the complex cepstrum to get the deconvolved wavelet. The channel response is deconvolved by Wiener filter shown in Figure 2.2.

Results and their interpretation

Figure 3.14--Figure 3.21 are the results of two-way simulation with different signal-to-noise ratios and different realization of random noise. The transmitted signal and the simulated channel response in these figures are the same. Figure 3.14--Figure 3.18 use the same realization of random noise (i.e., noise[a] of Figure 3.22) with signal-to-noise ratio from 2.787 dB to 0.1055dB. Figure 3.19--Figure 3.21 use another realization of random noise [b] of Figure 3.22. Figure 3.14, Figure 3.17, and Figure 3.19 show us the deconvolved channel response and minimum-phase wavelet under different received signal. The complex cepstrum of noise, transmitted signal, and channel response are shown in Figure 3.16 and Figure 3.21. The recovered signal and its cross correlation function with transmitted pulse is depicted in Figure 3.15, Figure 3.18, and Figure 3.20. These figures show that the center frequency of transmitted signal is rather well deconvolved down to a *SNR* of about 0 dB, and it seems relatively insensitive to additive noise. When the *SNR* is higher and the noise is quite 'white', the shape of the transmitted signal can also be deconvolved as presented in Figure 3.15. By comparing Figure 3.14 and Figure 3.16 with Figure 3.19 and Figure 3.21, we can see that the deconvolution of channel response is sensitive to

the 'whiteness' of noise. Same as in Figure 3.12, Figure 3.22 says that the larger the STD, the wider the complex cepstrum. The cepstrum of noise in Figure 3.21 is wider than the one in Figure 3.16, therefore, the resolution of channel response in Figure 3.19 is lower than that in Figure 3.14. However, both these figures demonstrate that the Wiener filter does well in increasing the resolution of the channel response estimation. Theoretically, the resolution of the processing depends on the bandwidth of the original signal. In simulation, the bandwidth of transmitted signal is 3kHz, so the resolution is 0.33(ms) which can be seen in Figure 3.14. Since the channel response of two way propagation is more complex than that of one way propagation, the complex cepstrum of channel response contributes not only the 'high time' of cepstrum but also the 'low time' of cepstrum. Thus the channel response cannot be deconvolved down to *SNR* of -11.65dB as with one way simulation. In Figure 3.17, when *SNR* equals 0.1055dB, we still can get the correct time delay of the signal to be send out and return along the shortest path. In addition, the transmitted signal is minium phased, so, in Figure 3.16 and Figure 3.21, the cepstrum of transmitted signal only occupies the positive part, which is consistent with Chapter 2.

The simulation results of one-way and two-way propagation show that the obvious advantage here is that the recovery method is independent of the original signal and the transfer function. Once some spectrum or cepstrum distribution characteristics of the transmitted signal or channel response is known, both of them can be deconvolved. Therefore, the deconvolution method detailed in Chapter 2 is robust to changes in the original signal or the transfer function due to the variations in the propagation channel. The processing is, however, sensitive to the whiteness of the additive Gaussian noise. As long as *SNR* is greater than 3dB after matched filtering, then recovering of the channel impulse response is possible, based on the simulation results shown here.

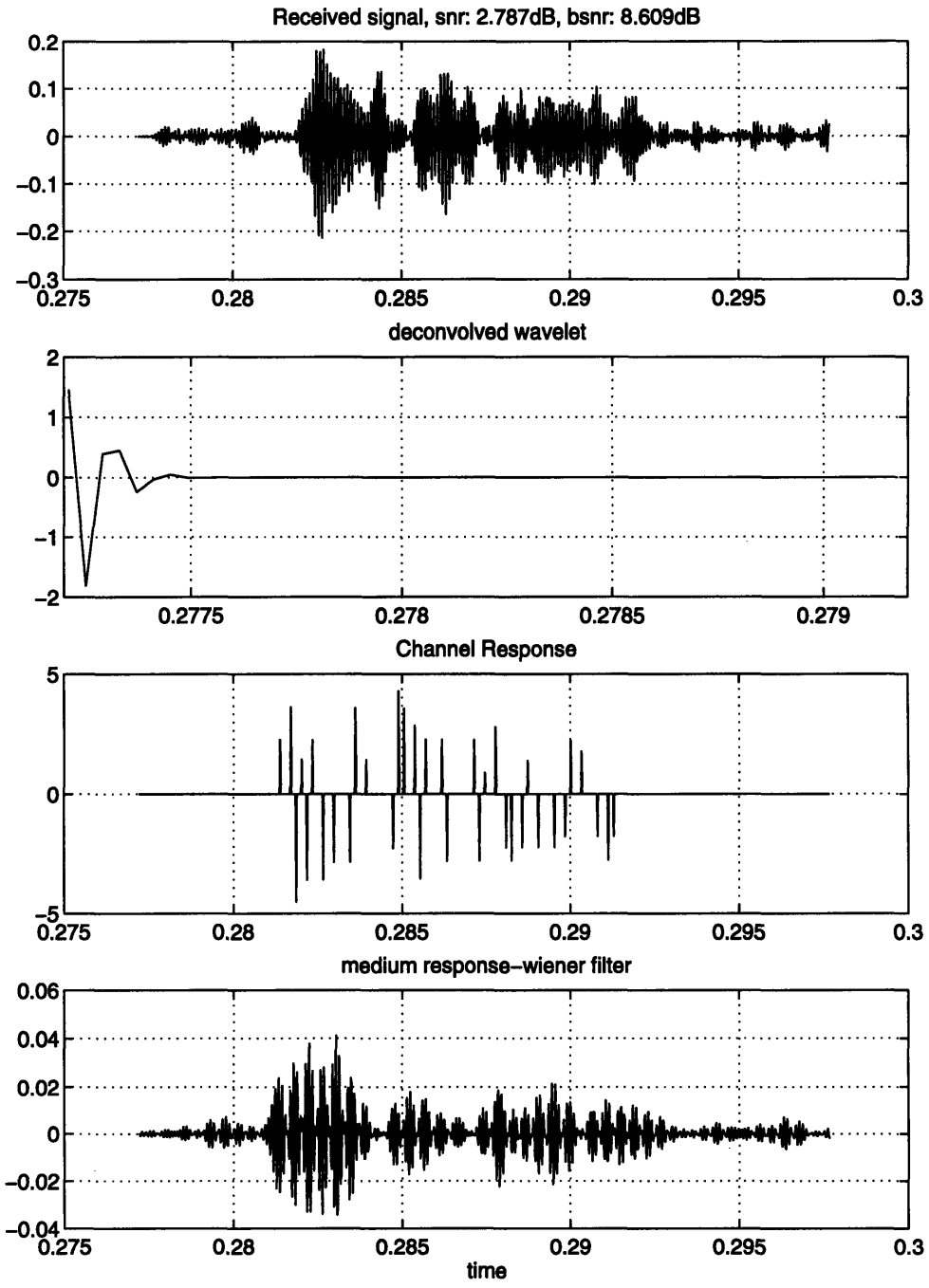

Figure 3.14: Deconvolution of channel response (two way)

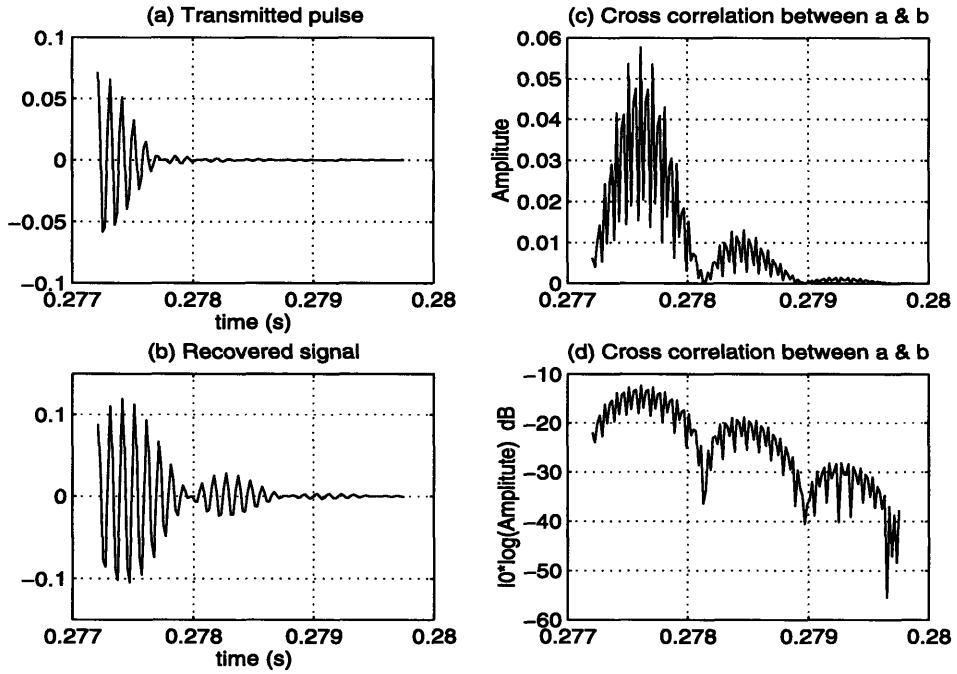

Figure 3.15: Comparison of transmitted signal and recovered signal [correspond to received signal of Figure 3.14]

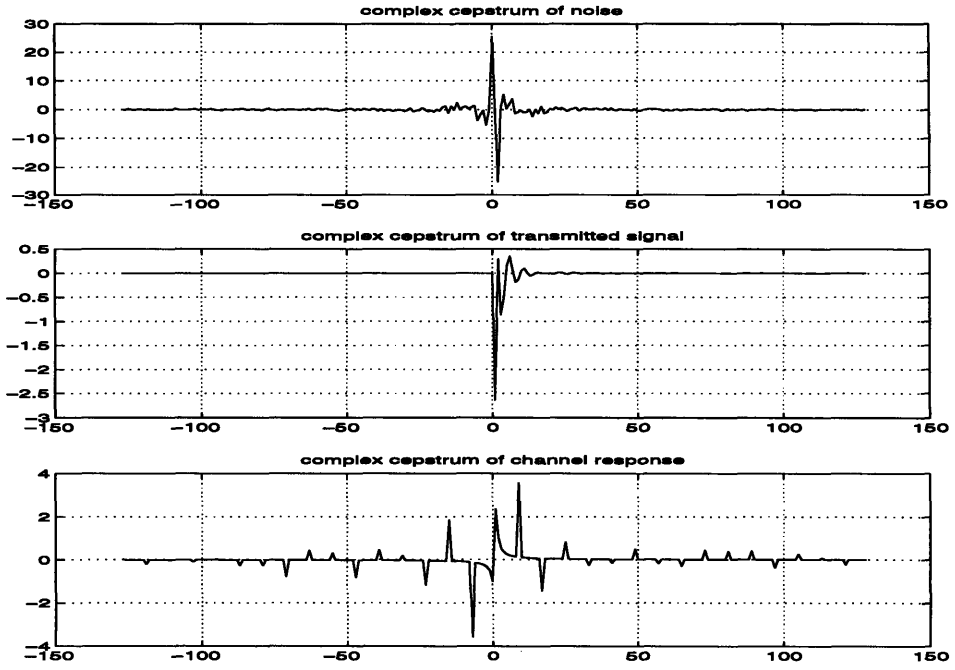

Figure 3.16: Complex cepstrum of noise, Transmitted signal and channel response [correspond to received signal of Figure 3.14]

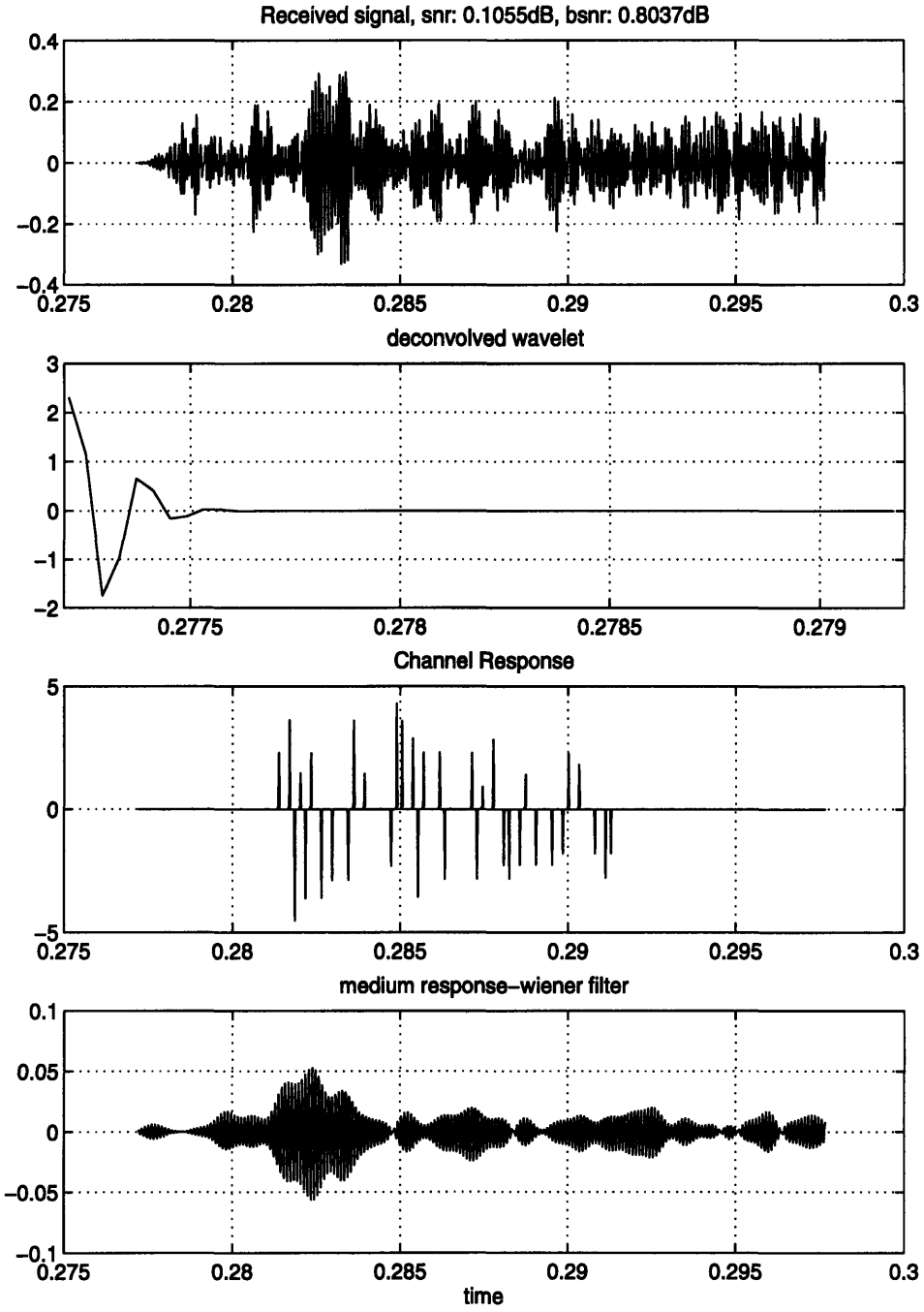

Figure 3.17: Deconvolution of medium response (two way)

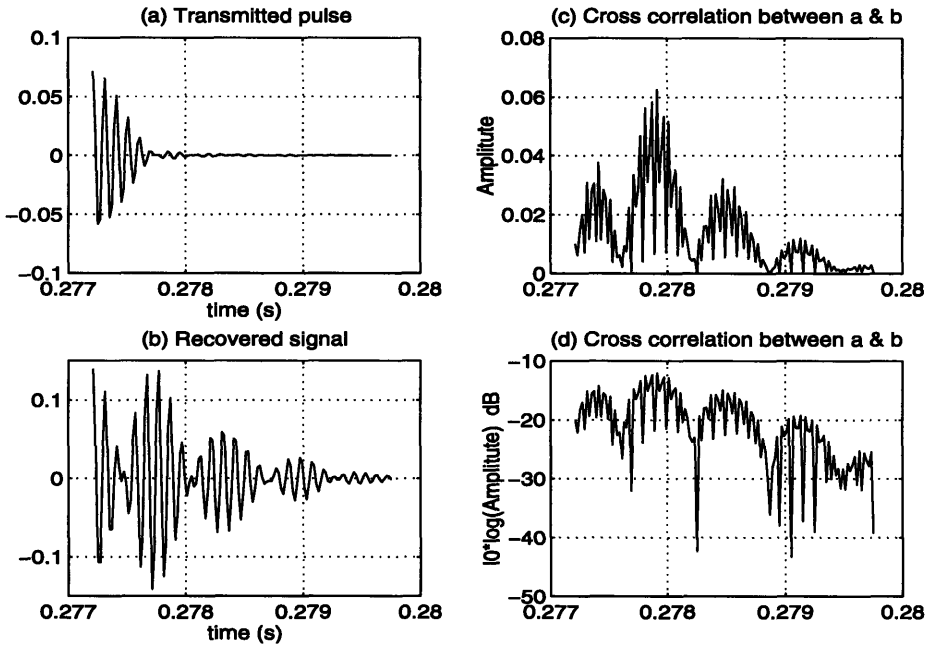

Figure 3.18: Comparison of transmitted signal and recovered signal [correspond to received signal of Figure 3.17]

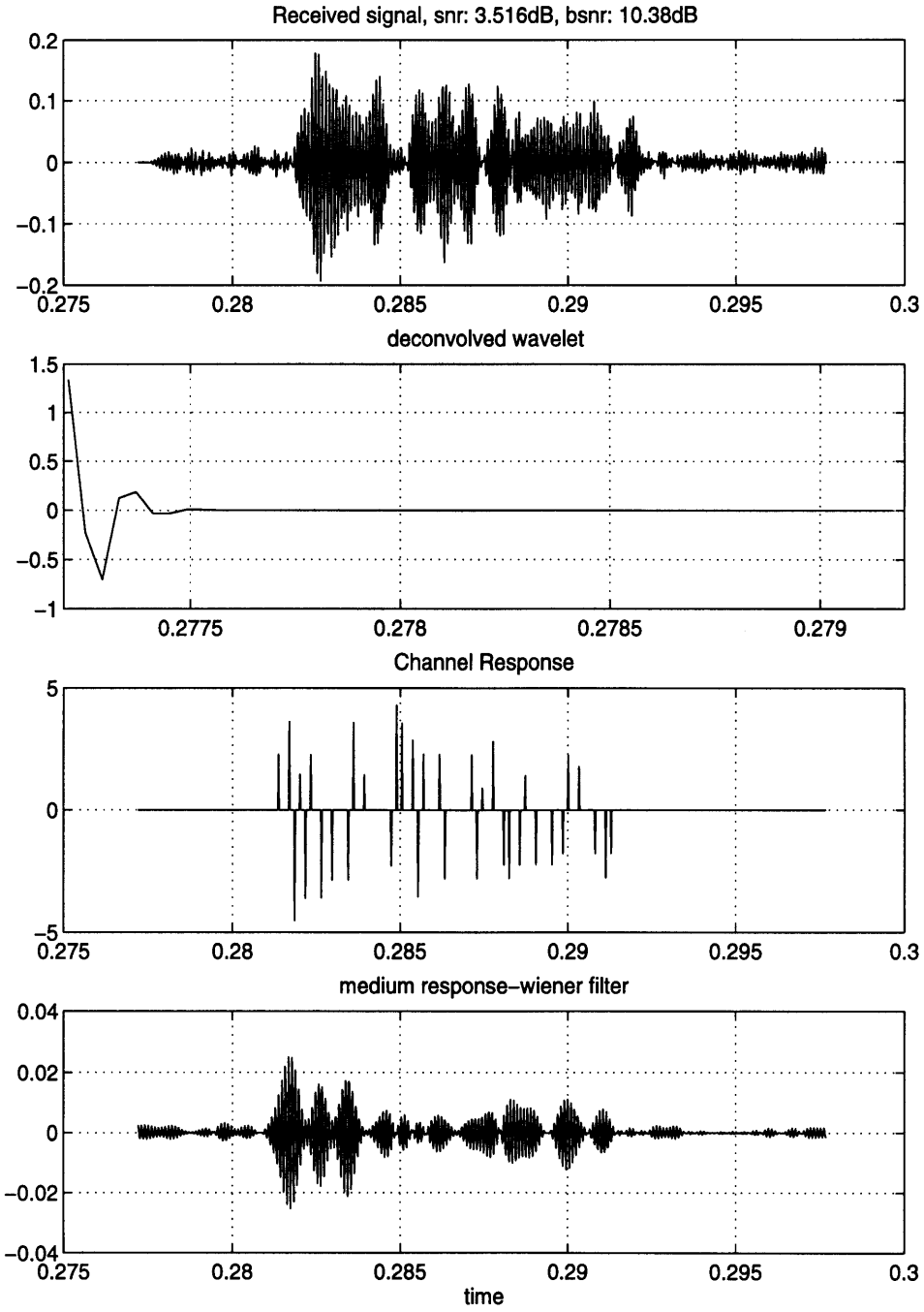

Figure 3.19: Deconvolution of channel response (two way)

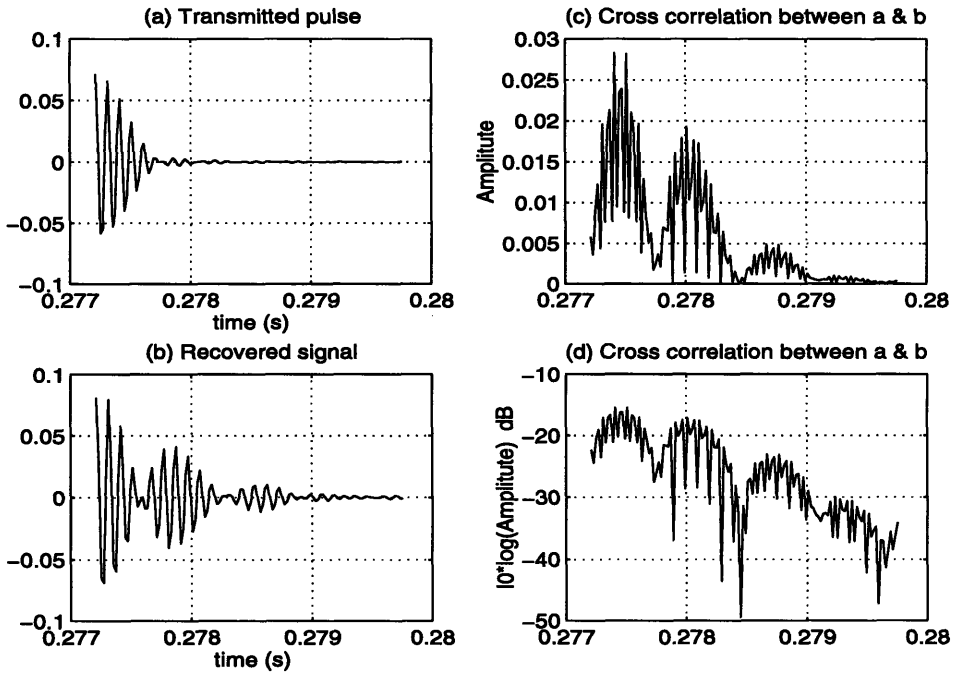

Figure 3.20: Comparison of transmitted signal and recovered signal [correspond to receive signal of Figure 3.19]

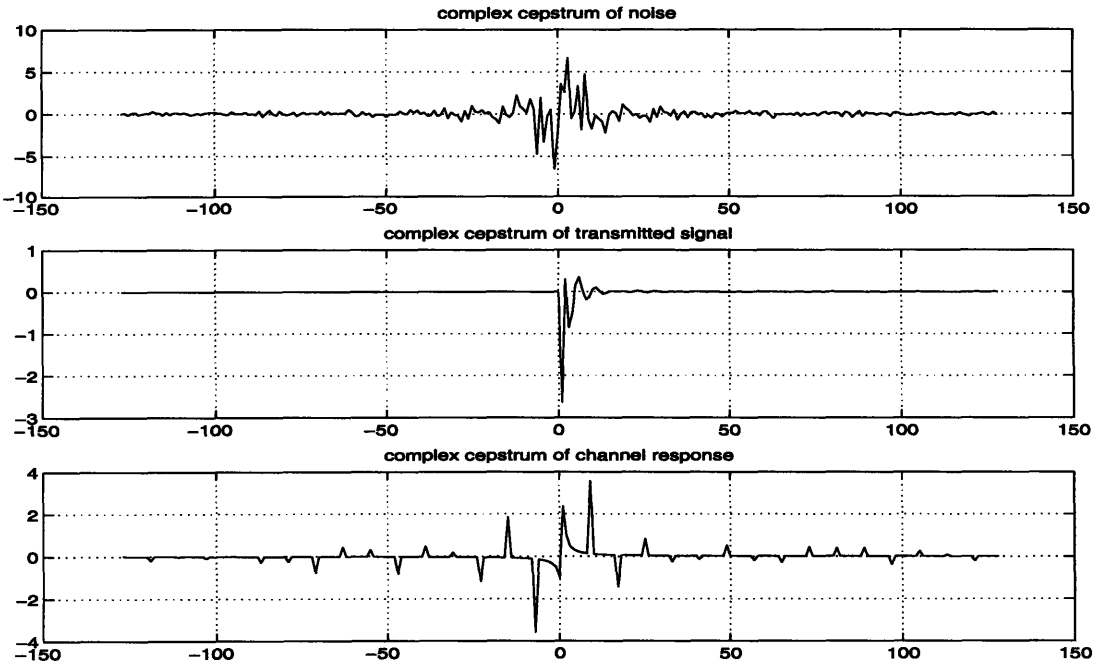

Figure 3.21: Complex cepstrum of noise, transmitted signal and channel response [correspond to received signal of Figure 3.19]

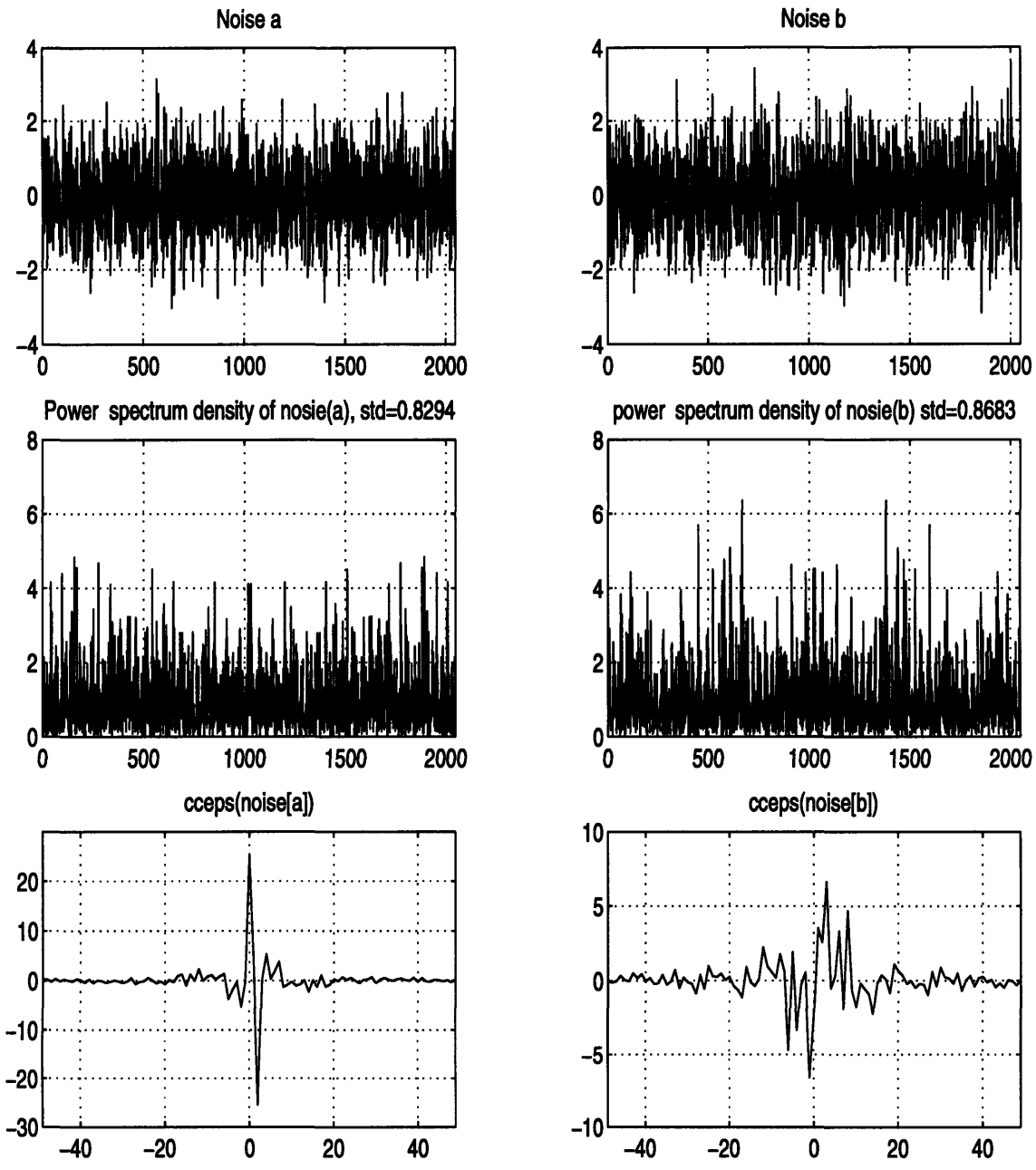

Figure 3.22: Comparison of two realizations of random noise

Chapter 4

Results with experimental data

4.1 Recovery of medium response

Experimental condition

The field data discussed here came from an acoustic reverberation experiment conducted by Draper Laboratory. The aim of the experiment was to estimate the multipath structure and to detect targets near the shallow water bottom. The experiment scenario is depicted in Fig. 4.1.

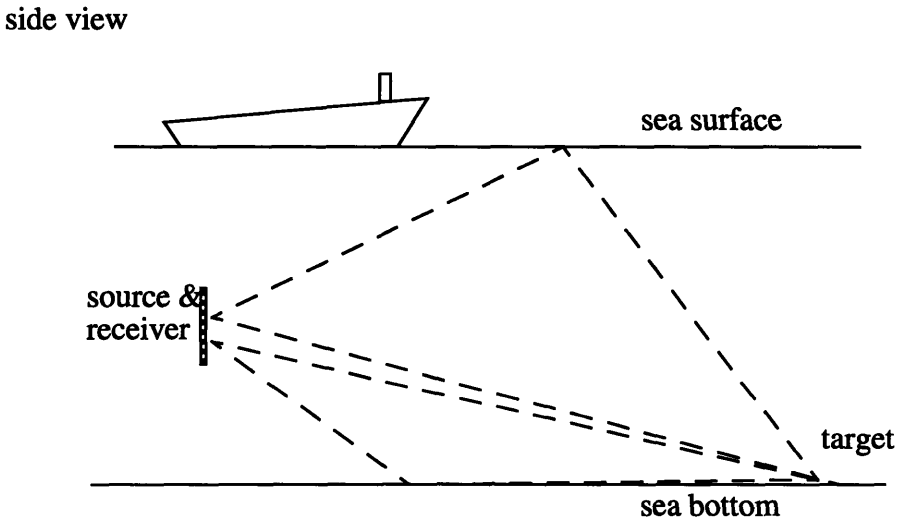

Figure 4.1: Configuration of backscattering experiment

The source and the receiver were co-located with the source approximately 2 feet below the receiver array. The source was at a depth of approximately 22 feet, while the bottom depth was approximately 40 feet. The source array is omni-direction and the receiver array has a vertical beamwidth of about 20 degrees while the horizontal beamwidth is 11.25 degrees steering from 202.5 degrees to 337.5 degrees. The azimuthal angle of the receiver array in the horizontal is bearing-oriented, with forwarded being 0 degree,

starboard beam 90 degrees, aft 180 degrees, and port beam 270 degrees. The receive array is designed to be populated with hydrophones only on the port side, hence the range of beam centers from 202.5 to 337.5 degrees all refer to the port side as well. The sound velocity profile at a nearby mooring is depicted in Figure 4.2, where the star and cross represent the source and the receiver, respectively.

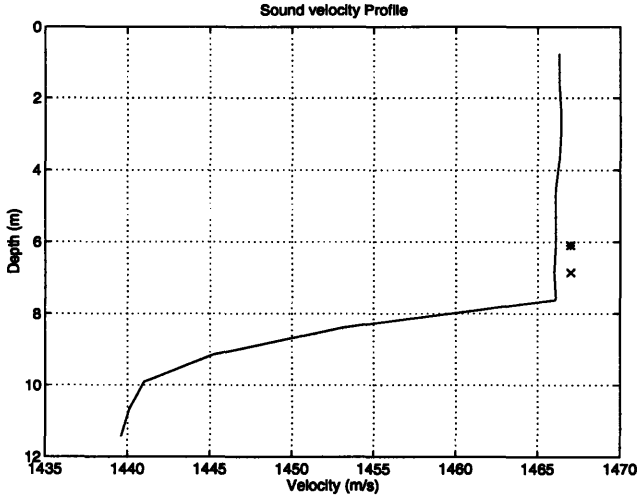

Figure 4.2: Sound velocity profile

Signal characteristics

An FM chirp was used for the experiment with a center frequency of 8.5 kHz and a bandwidth of either 5 kHz or 7kHz, and a duration of 5, 10, 20, or 40 msec, depending on the ping as shown in Table 4..1.

Ping number	Duration	bandwidth (Hz)
526,531,536	5msec	5000
527,532,537	10msec	5000
528,533,538	20msec	5000
529,534,539	40msec	5000
530,535,540	40msec	7000

Table 4.1: Duration and bandwidth of Ping signal

The barge moved due north following a line. The ping number corresponds to the dif-

ferent points on the line. The x-y positions in meters of the array for pings 526 to 540 are shown in Table 4.2.

526 [2346.3m, 1725.3m]	531 [2352.1m, 1735.9m]	536 [2347.1m, 1749.4m]
527 [2347.7m, 1727.9m]	532 [2351.7m, 1738.8m]	537 [2346.3m, 1754.0m]
528 [2349.0m, 1730.3m]	533 [2350.5m, 1741.3m]	538 [2345.9m, 1758.3m]
529 [2350.5m, 1732.9m]	534 [2349.3m, 1743.7m]	539 [2345.2m, 1761.4m]
530 [2351.7m, 1734.2m]	535 [2347.8m, 1745.9m]	540 [2344.7m, 1764.2m]

Table 4.2: Position of different ping

Description of the processing

Beam time series data is roughly 325m, which corresponds to 11265 range bins. All the receiver signals have been matched filtered and are processed with the same steps detailed in Figure 2.2. Due to the computer memory limitation, the received signal first passes the moving window, which also depresses the noise outside it, and thus improves the signal-to-noise ratio. The wavelet is deconvolved by the complex cepstrum (after band-pass mapping). The channel response is resolved by Wiener filtering.

Results

The received time series, the deconvolved channel responses and their spectrums for ping number 526, 527, 528, 529, and 530 are depicted in Figures 4.3, 4.5, 4,7, 4.9, 4.11. The deconvolved wavelet, the resolved transmitted signal and its spectrum of different moving window are show in Figure 4.4, 4.6, 4.8, 4.10, 4.12. Comparing (a)'s and (b)'s of Figures 4.3, 4.5, 4,7, 4.9, 4.11, we can see that the Wiener filter really gives us a sharpened channel response. Since the bandwidth of the transmitted signal is 5000 Hz and 7000 Hz for different pings (seen Table 4.1), the theoretical resolution is, respectively, about 0.144 m and 0.1029 m, if we assume a sound velocity is 1440 m/s. The difference of recovered signal spectrum at different moving window is mainly caused by the *SNR* of that window

which has been discussed in chapter 3.

All of these figures show that the method detailed in Figure 2.2 is helpful in increasing the resolution of channel response, which is the key basis to detect the targets, because the channel response can be thought of as the convolution of target information with channel information. In the next section, we will discuss how to sharpen the image and remove spurious detections caused by multipaths.

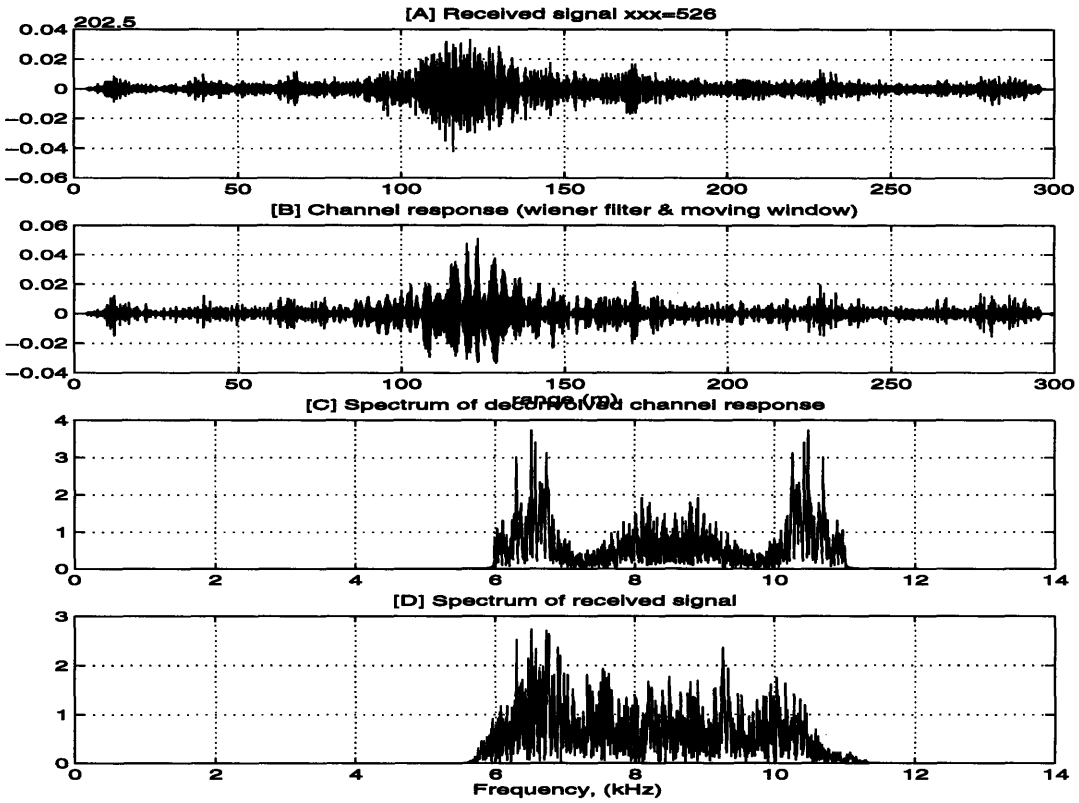

Figure 4.3: Received signal and deconvolved channel response

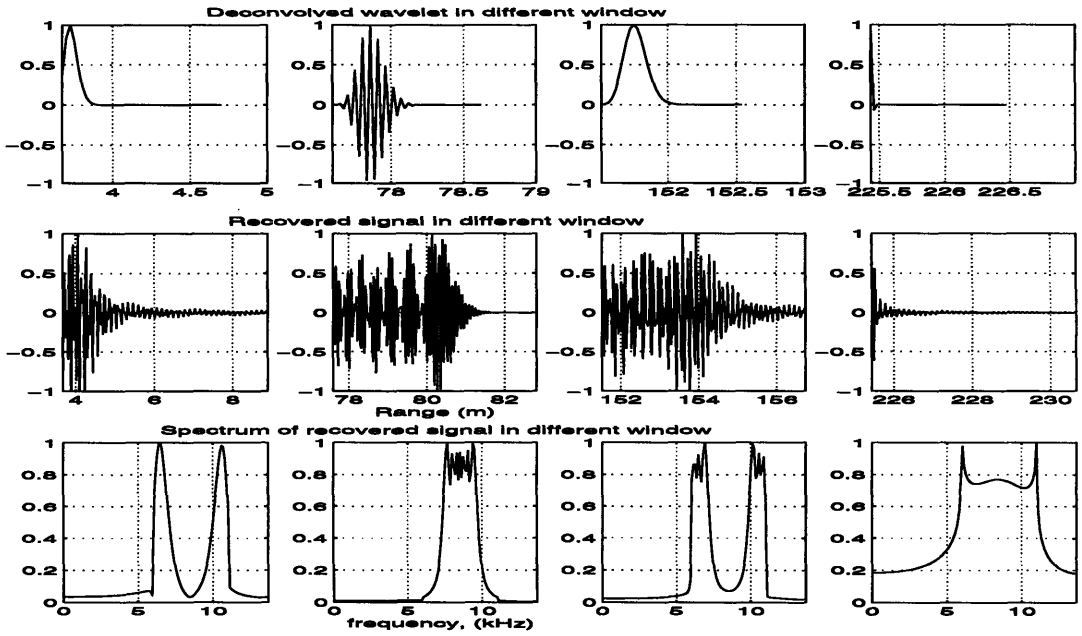

Figure 4.4: Deconvolved wavelet and recovered signal (same received signal of Fig 4.3)

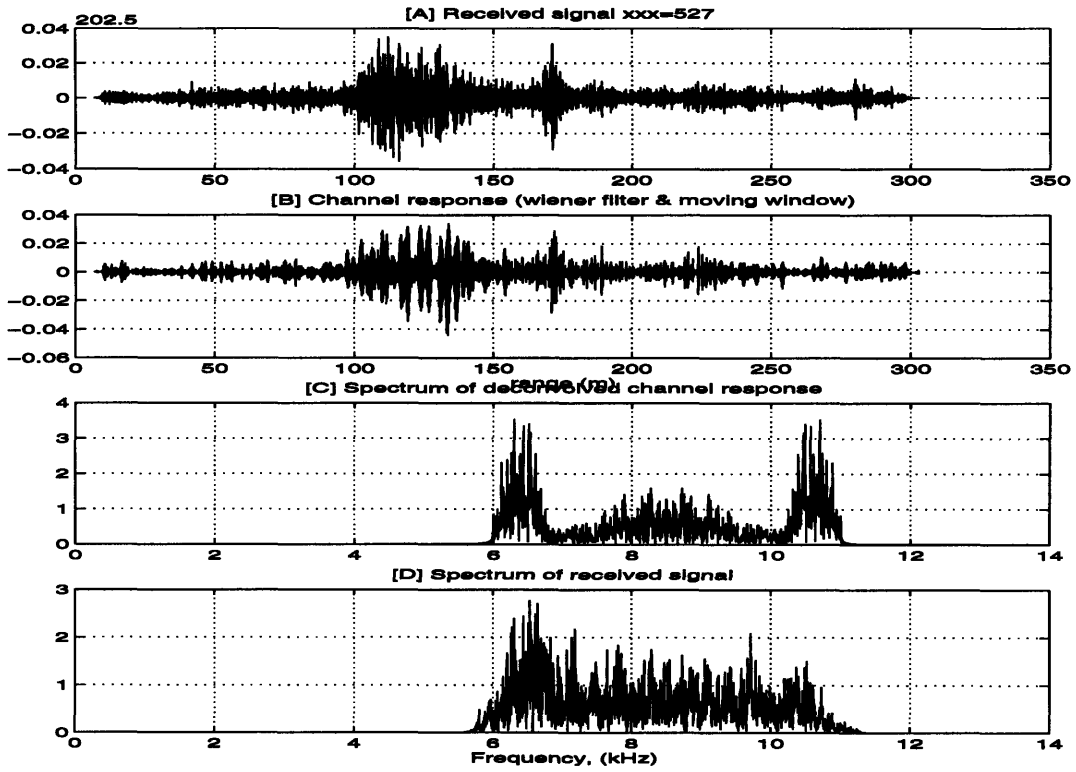

Figure 4.5: Received signal and deconvolved channel response.

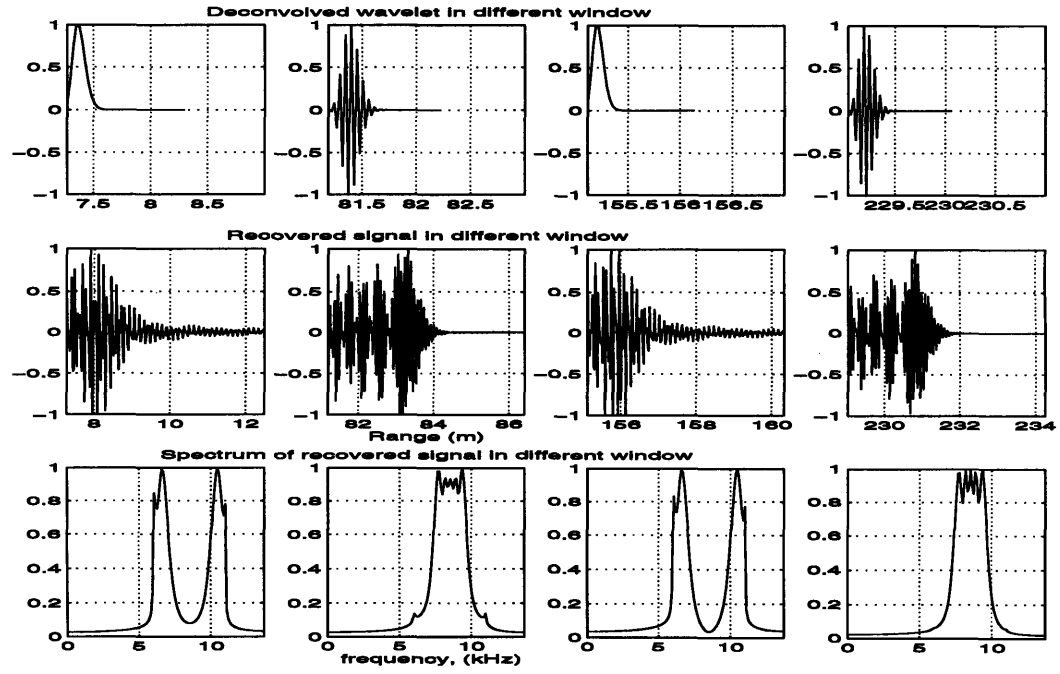

Figure 4.6: Deconvolved wavelet and recovered signal (same received signal of Fig 4.5)

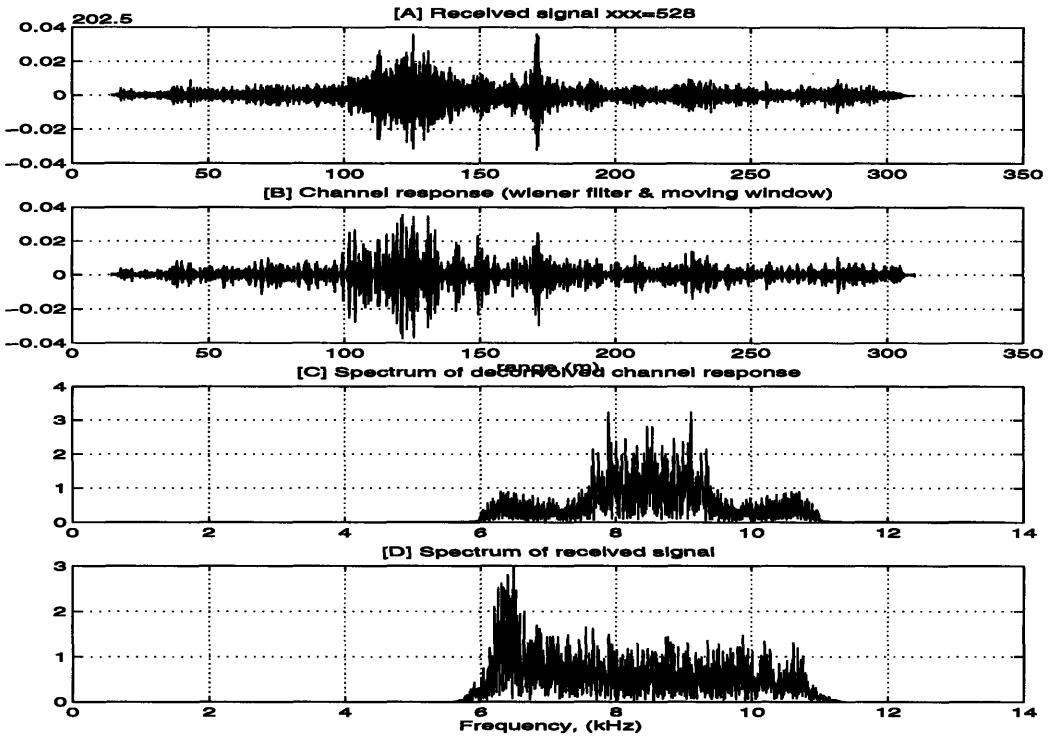

Figure 4.7: Received signal and deconvolved channel response

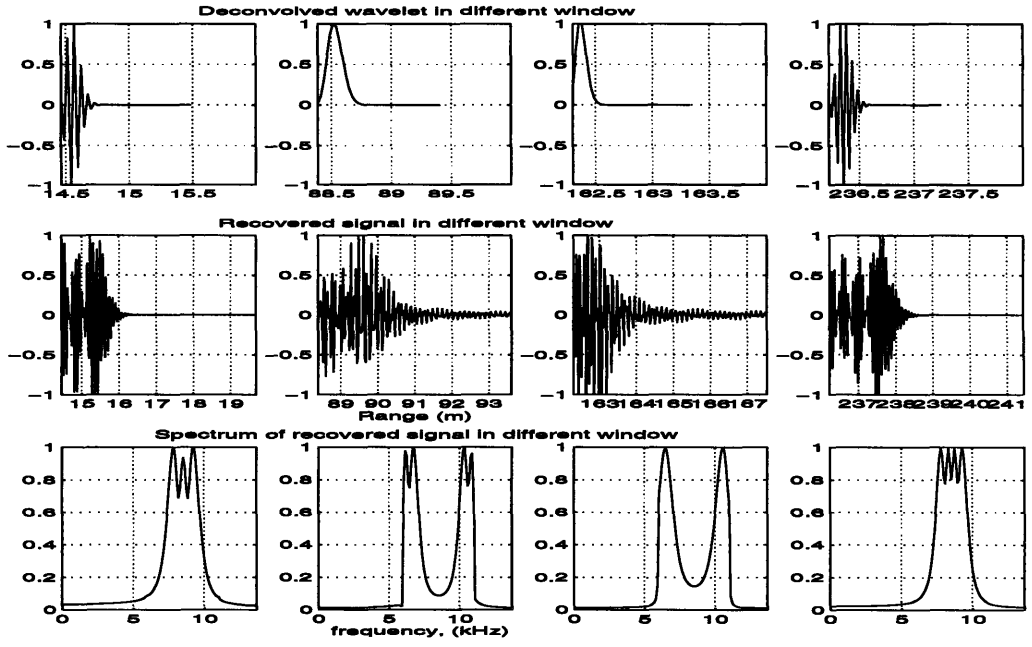

Figure 4.8: Deconvolved wavelet and recovered signal (same received signal of Fig 4.7)

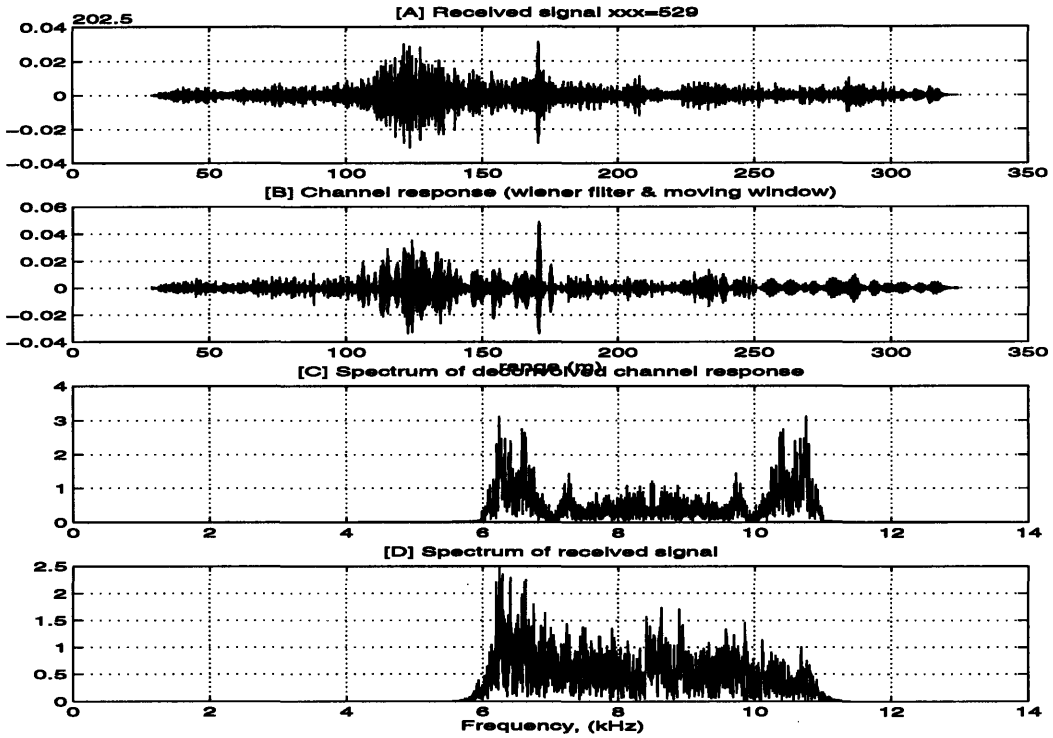

Figure 4.9: Received signal and deconvolved channel response

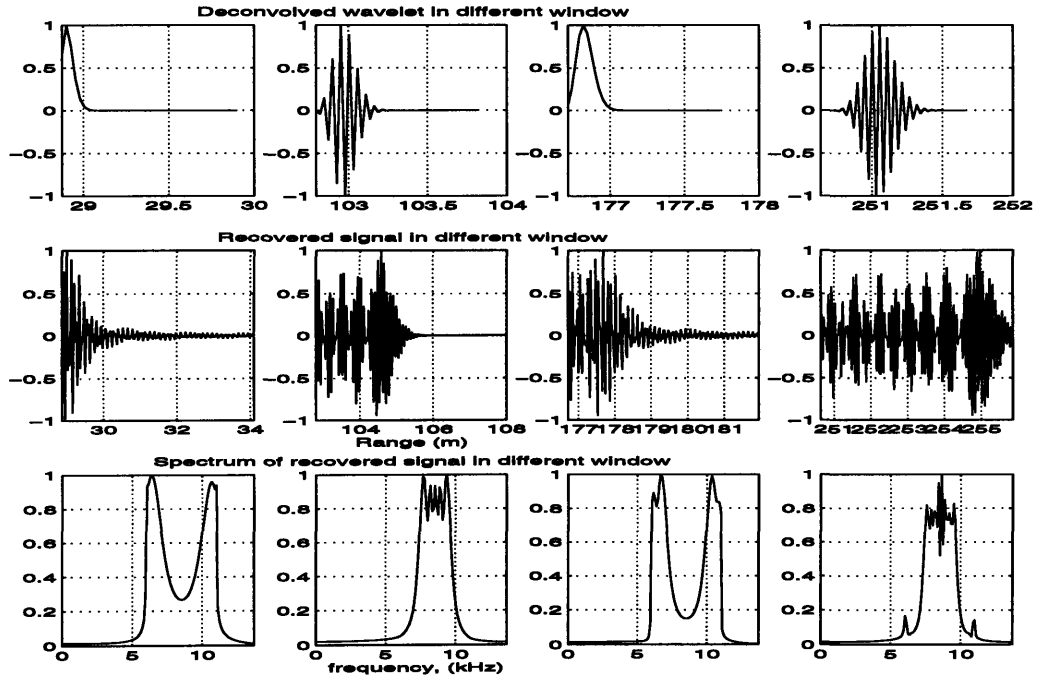

Figure 4.10: Deconvolved wavelet and recovered signal (same received signal of Fig 4.9)

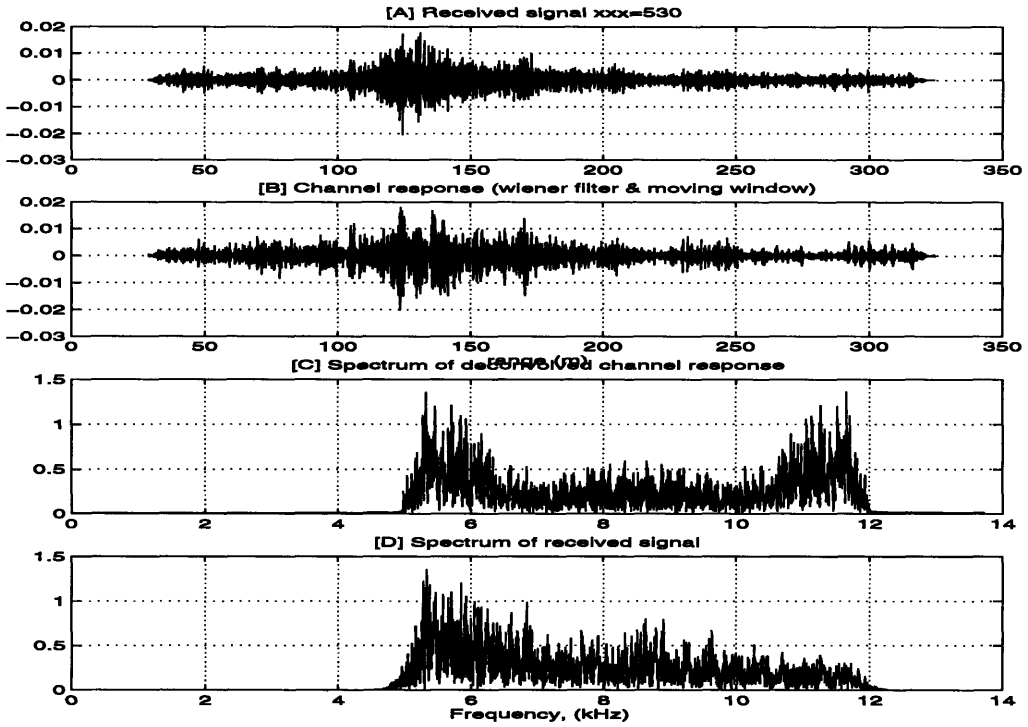

Figure 4.11: Received signal and deconvolved channel response

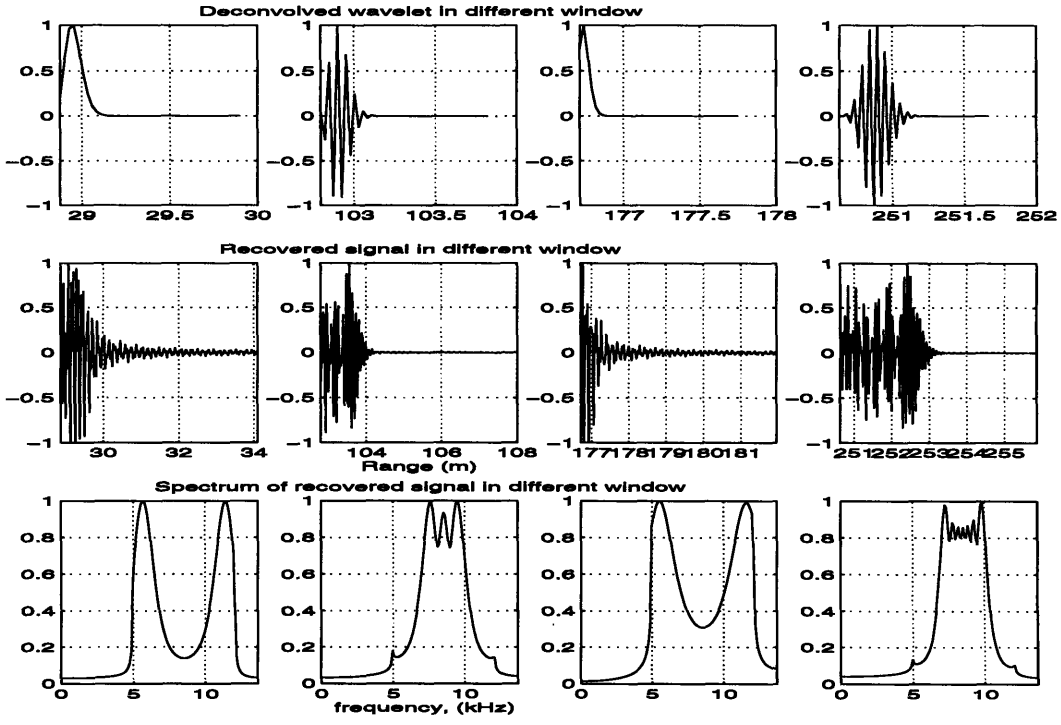

Figure 4.12: Deconvolved wavelet and recovered signal (same received signal of Fig 4.11)

4.2 Target detection

In section 4.1, we have already gotten the sharpened channel response at different directions of different ping numbers, which correspond to the navigation points. Base on that, we can use information of both amplitude and phase to find the target distribution free of multipaths. Following are three aspects of target detection.

B-scan map

With all the amplitude information, B-scan maps give some intuition of target distribution in range scale. Let the ping position be the centre of a circle, the same range bin of 13 direction beams must be on the same radius of a circle, so, the maximum value of one range bin between 13 direction beams of one ping must contain some information of the target if there exists targets near that range bin. Therefore, the first step is to get the 'maximum value beam' from 13 direction beams of one ping, then put all the 'maximum value beams' together to get Figure 4.12. Both figures of Figure 4.12 are drawn with data integrated from the processed experimental data because of computer memory limitation. One point of the top figure is integrated with 16 points which equal 0.42m, and one point of the bottom figure is integrated with 44 points which equal 1.155m. There is not much difference between these two figures. That is to say, the error caused by integration is in the range of experimental error. Figure 4.13 also tell us that the power of the received signal decreases as the bandwidth of the emitted signal increases. In order to cut off the interference of power of 'maximum value beam', the technique of AGC (automatic gain control') is used to get Figure 4.14 so that many points with low *SNR* (dark color) in Figure 4.13 can be seen in Figure 4.14. Both Figure 4.13 and Figure 4.14 are generally called B-scan maps, which condenses all the data into one figure. It can be seen from these figures that the candidate targets are identified at range of around 120m, 175m, and 230m for ping #77.

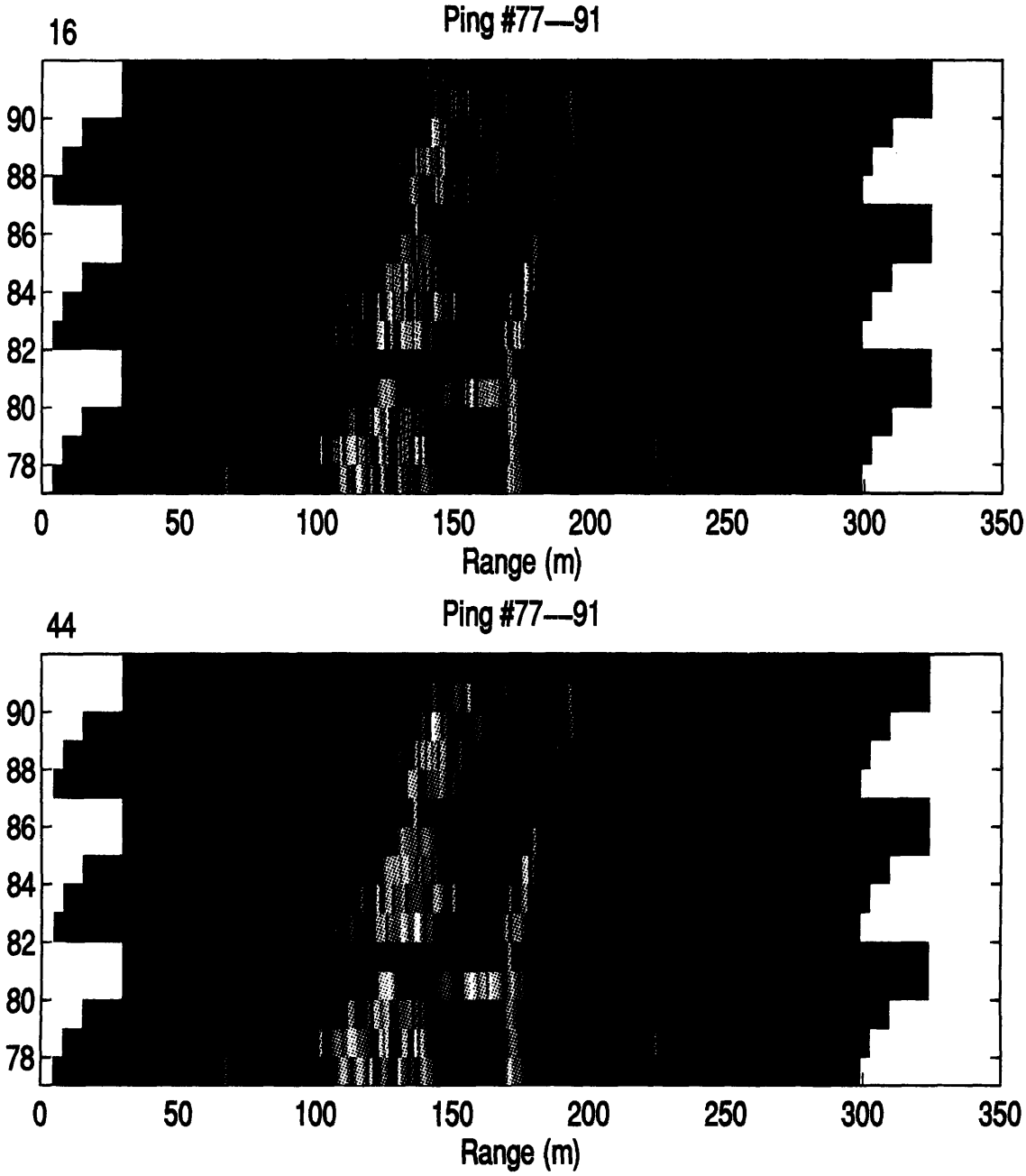

Figure 4.13: B-scan map

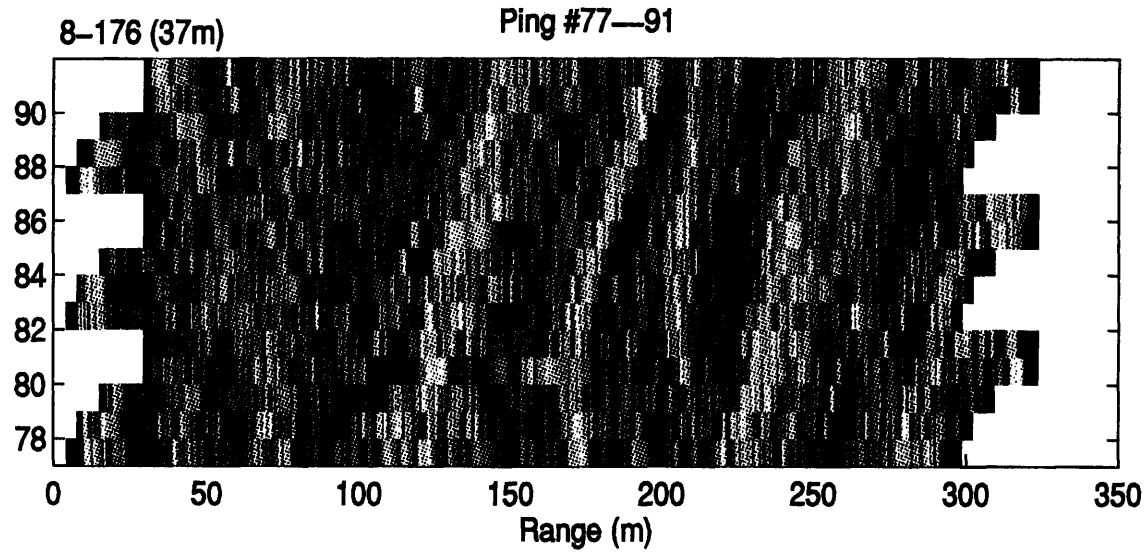

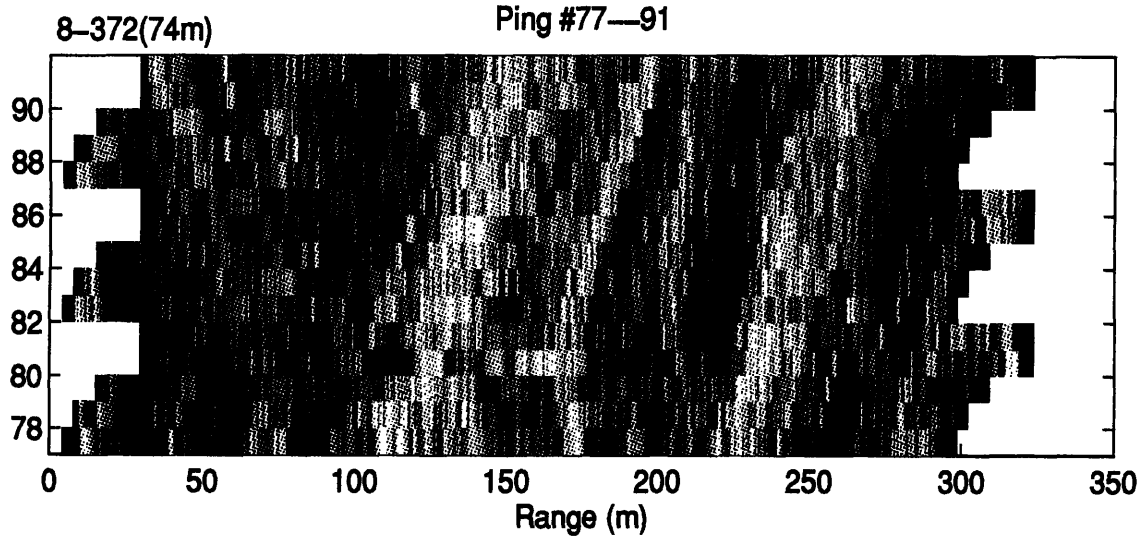

Figure 4.14: B-scan map

Target Localization

Target localization presents the real geometric distribution of targets using amplitude and azimuthal angle information. As the barge moves on, the spurious targets caused by multipaths will change their positions in a coordinate with respect to a fixed point on the land while the real targets' positions remain unchanged. With this idea, we smooth the deconvolved channel response to obtain the waveform, then set a threshold level to filter the targets, and finally locate their positions according to time delays, positions of pings, and angles of beams, in a coordinate with respect to a fixed point. Since, the resolution of the channel response achieved by Wiener filter is increased, we will be able to detect the weak target near strong objects if we lower the threshold. From Figure 4.15-4.16, the direction distribution of targets can be seen obviously: most of the strong targets are along the aft direction of barge while the weak targets are along the forward direction of barge. This phenomenon may be caused by the steep sloping bottom. The relationship between the signal power and bandwidth can also be observed in these 'target maps'. Those points which overlap each other can be thought as the 'most likely targets', which are also shown in the bright color area of the B-scan picture (around 120-150m).

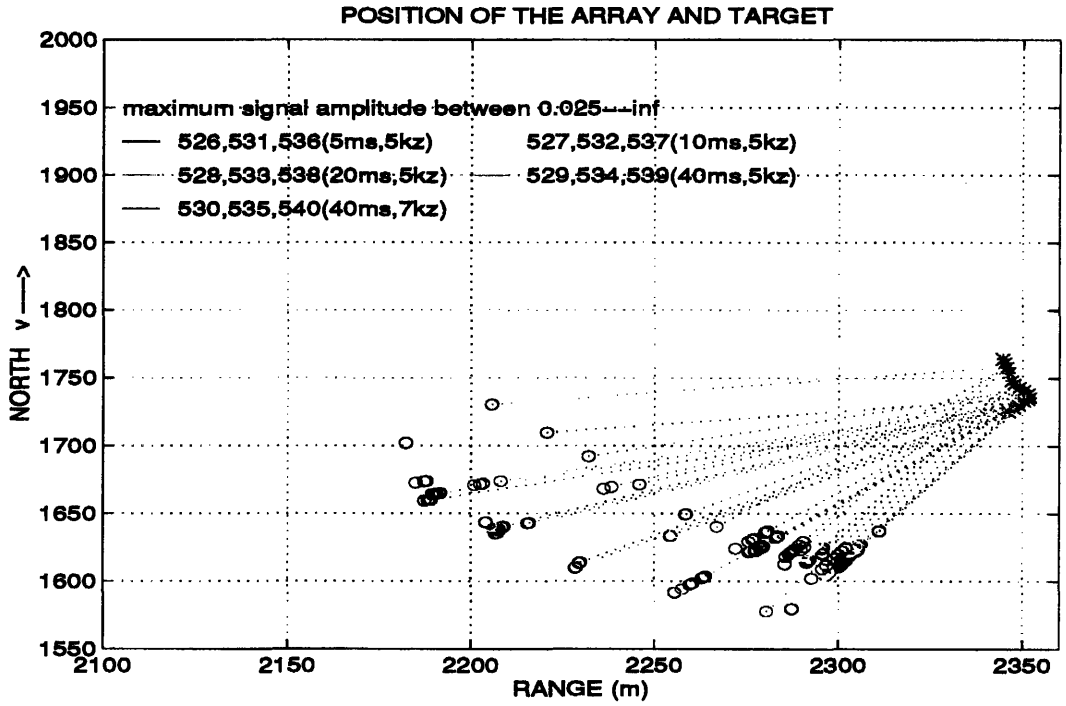

Figure 4.15: Target map of high amplitude signal

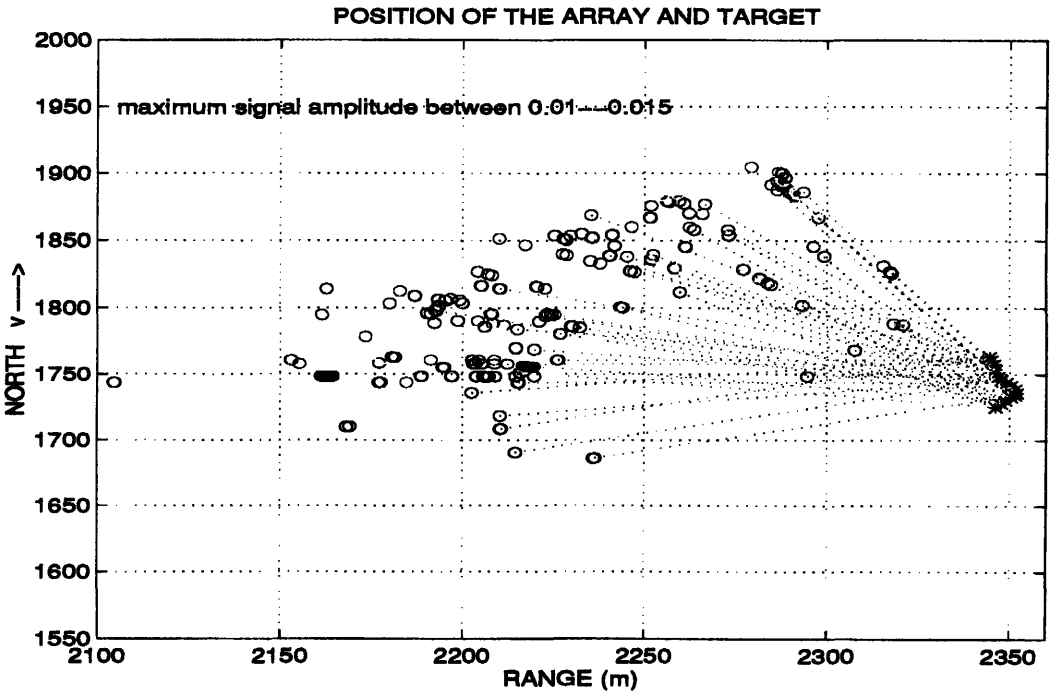

Figure 4.16: Target map with low amplitude signal

Excess path lengths due to multipath

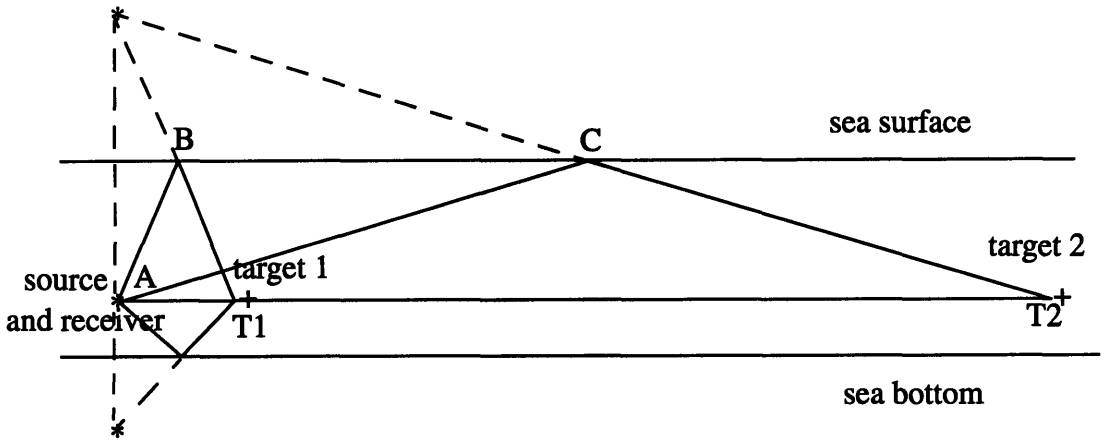

Figure 4.17: Multipath and direct path

The excess path length, also called apparent additional range, is the difference between multipath and direct path. From Figure 4.17, we can see that the 'excess path length' will decrease as the distance between the target and the source increases. Suppose the target is at an infinite distance, then the 'excess path length' equal zero, which means there is no range difference between the direct path and the multipath. So, if we can find this kind of structure of multipath from the experimental data, we can decide which kind of multipath (reflective or refractive) is dominant under shallow water in this experimental area and find the target position by comparing with the theoretical result. Figure 4.18-4.19 show that the similar 'excess path length due to multipath' relation is obvious from the channel response after applying the Wiener filter while it is difficult to see this relation from the original received signal. Since the experimental range is short, the theoretical result with iso-velocity profile shown in Figure 4.2 can be use as the result of real sound velocity profile. In order to get the 'excess path length' from real data, we first apply the rectangular window to the deconvolved channel response. The window length should be greater than the longest 'excess path length' chosen from Figure 4.20 according to the dif-

ferent range points. Then autocorrelate the time series inside the window. Finally, the time delay between the peaks of time series after autocorrelation corresponds to the 'excess path length' near that range. The experimental result of one beam data was depicted in Figure 4.21 in which the light color depicts the peak and the dark color represents valley. Comparing Figure 4.20 with Figure 4.21, we conclude that the multipath structure named 'excess path length due to multipath' can be obtained from the deconvolved channel response which confirms that the method detailed in Figure 2.2 improves the resolution.

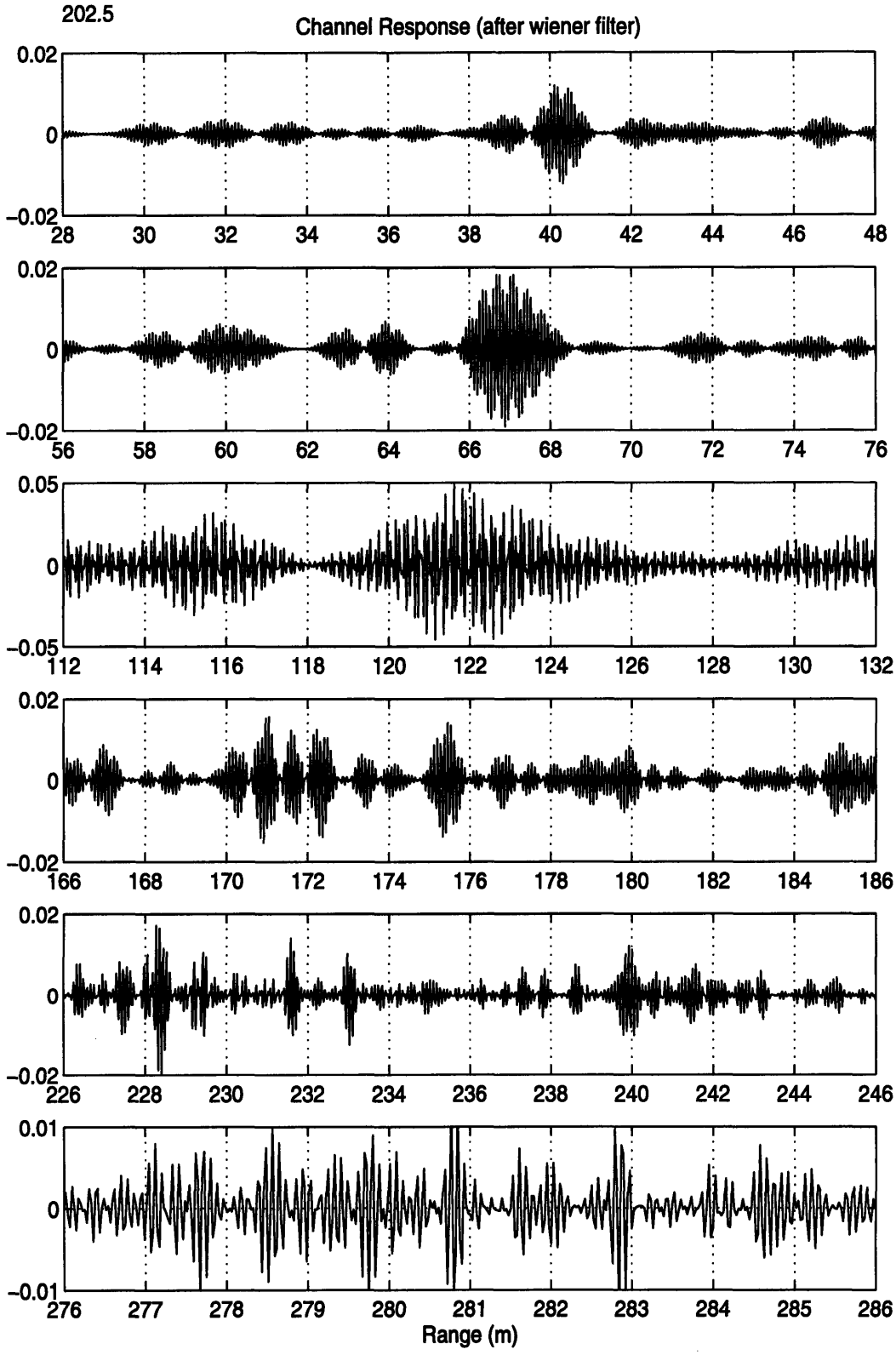

Figure 4.18: Deconvolved channel response

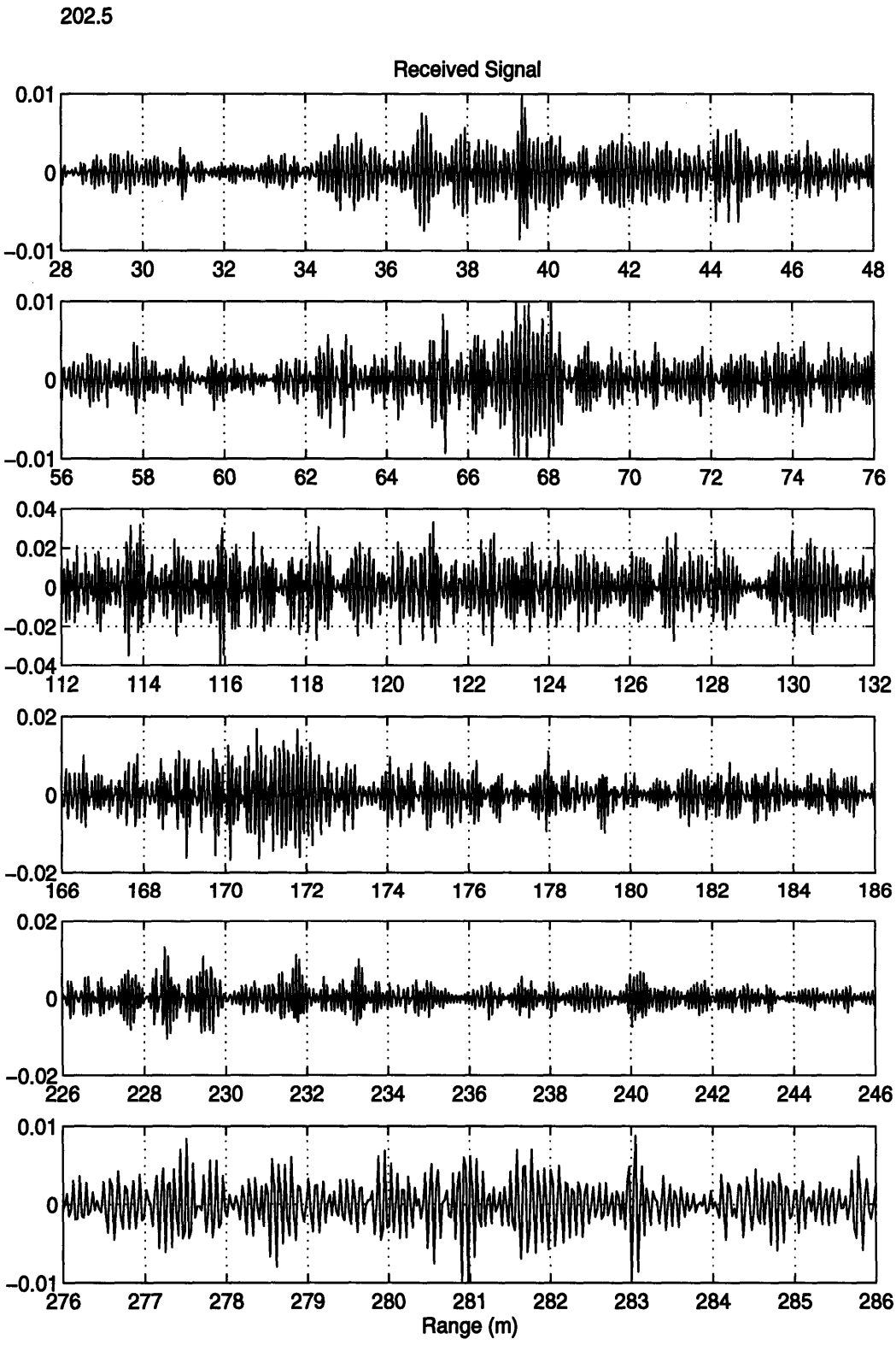

Figure 4.19: Received signal

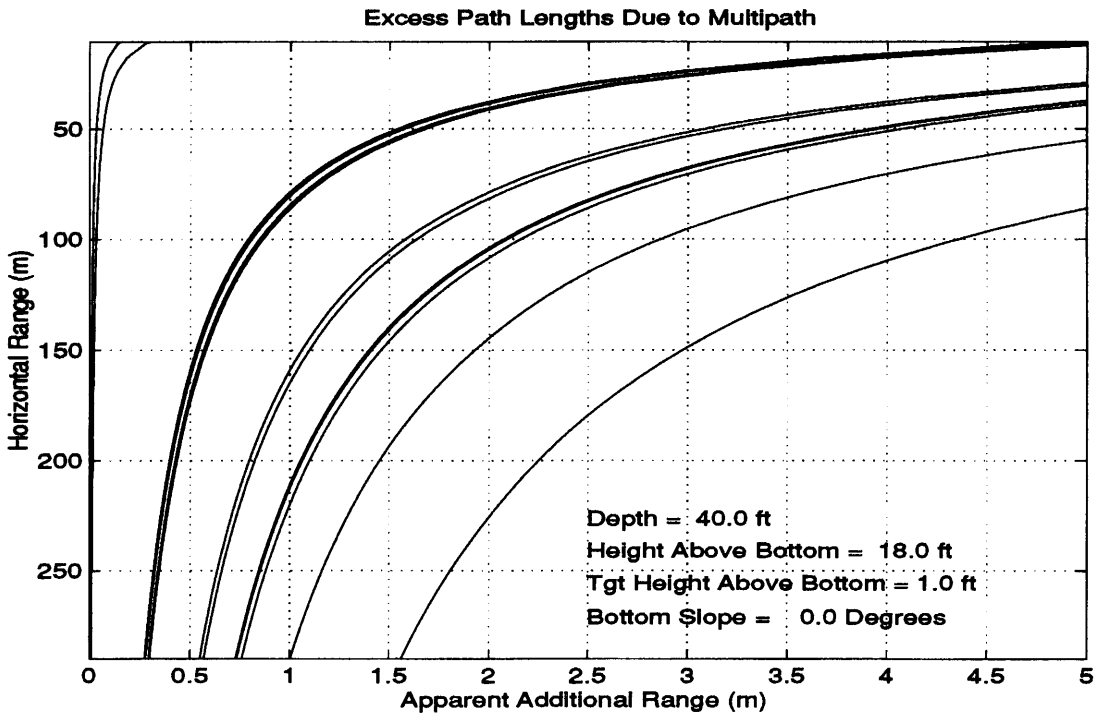

Figure 4.20: Excess path length from theoretical calculation

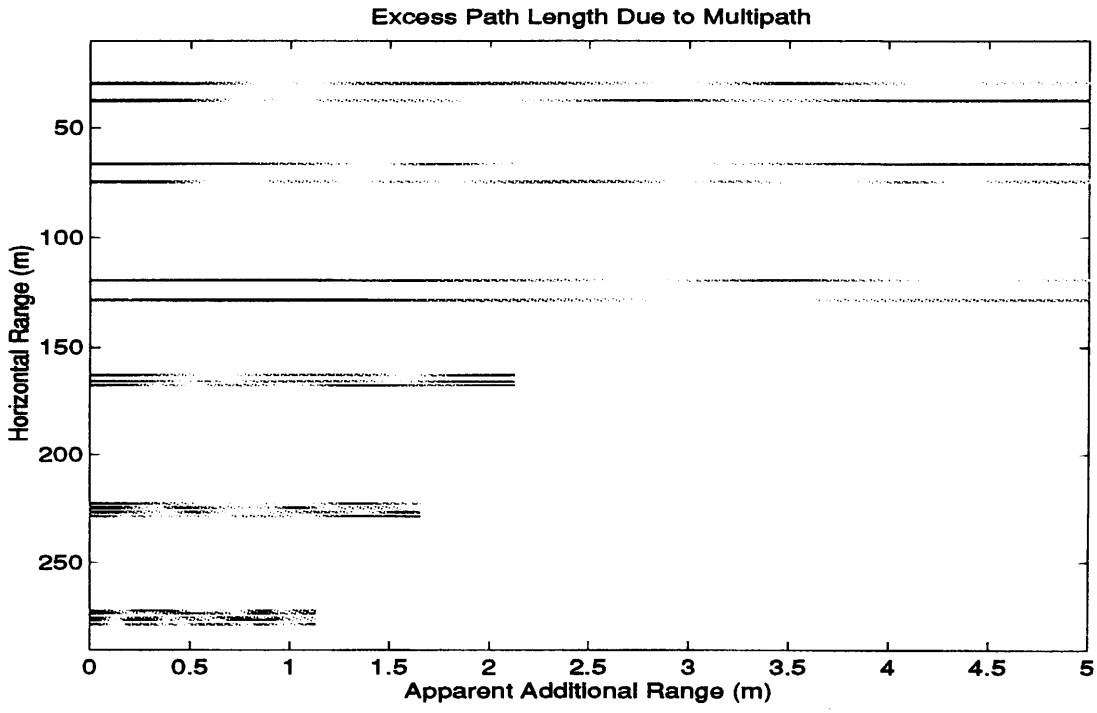

Figure 4.21: Excess path length from experimental data after Wiener filter

Chapter 5

Conclusions

In this thesis, the synthetic data of both one way and two way propagation has been analyzed to successfully recover the sonar signal and the channel response from the received signal, which is corrupted with both ambient and reverberant noise (chapter 3). Substantial improvement in increasing the resolution of channel response is demonstrated with Draper's field data. This makes possible the implementation of the 'target localization' and the 'excess path length' which is used as a filter to the data to analyze the effect of multipath. The method of B-scan maps is used to give some intuition of the targets distribution in the range scale.

The complex cepstrum used to deconvolve the wavelet does not require a minimum or maximum phase characteristic for the signals, and therefore is very useful in propagation and reverberation application, for which the signals are mostly mixed phase. Meanwhile, the complex cepstrum in this thesis is also used to separate the minimum phase and the maximum phase component to construct the causal and anticausal Wiener filter. Although the complex cepstrum requires a relatively high signal-to-noise ratio due to its phase being sensitive to the noise, it casts few effects in channel response recovery because we only use its property to transform the convolution in time to addition in the cepstrum domain. All the phase information is recovered by convolution of received signal with the constructed Wiener filter.

The combination of homomorphic deconvolution and Wiener filtering proves to be quite robust to the noise in that it capitalizes on the individual advantages of both the techniques. The homomorphic deconvolution handles the mixed phase characteristics of the

signal while the Wiener filter provides high resolution of the medium response. The method detailed in Figure 2.2 is successfully used for *SNR* down to -11.64 dB of one way propagation, and 0.2 dB of two way propagation. Some results using this promising mixed technique are demonstrated with experimental data through the 'B-scan map', the 'target localization', and the 'excess path length due to multipath'.

The 'target localization' and the 'B-scan' map are helpful for understanding the targets spatial distribution, which reflects the geological characteristics of the ocean environment. Thus, the intuition about how to extend the usable range of a sonar in shallow water can be obtained. The structure of 'excess path length' gained from the experimental data is beneficial for a better understanding of multipath, especially in shallow water. Therefore, it might be used as a filter to remove the spurious detections caused by multipath.

Work in the immediate future will focus on our more detailed testing of using the 'excess path length due to multipath' to find the true echo from an object to be observed free of multipath. Although the Wiener filter is quite successful in increasing the resolution of the channel response, it is not optimal for the uncorrelated noise and uncorrelated channel response, which limit its applications. An interesting extension of this work would be to find a filter which is effective in non-white environment.

Appendix A

Estimation of $R_{nn}(0)/R_{rr}(0)$

A.1 Likelihood function

Let matrix $S = (S_1, S_2, \ldots, S_M)$ be a series of independent, zero-mean, Gaussian random vector, where S_k is a series of random variables of order p, i.e.,

$$S_k = \begin{bmatrix} s[0] \\ \circ \\ \circ \\ s[p] \end{bmatrix}, k \in 1, 2, \ldots, M,$$

and $R_{ss} = R_{nn} + R_{yy} = R_{nn}(0)I + R_{yy}$.

The probability density function of S is given by

$$p(S/R_{nn}(0), R_{yy}) = (2\pi)^{(-MP)/2}|R_{ss}|^{-M/2}\exp\left(-\frac{1}{2}\sum_{k=1}^{M} S_k^T R_{ss}^{-1} S_k\right).$$

Define the likelihood function as

$$\Phi(S) = \frac{-2}{M}\ln p(S/R_{nn}(0), R_{yy}) - p\ln 2\pi$$

$$= \ln|R_{ss}| + \frac{1}{M}\sum_{k=1}^{M} S_k^T R_{ss}^{-1} S_k = \ln|R_{nn}(0)I + R_{yy}| + tr\left[(R_{nn}(0)I + R_{yy})^{-1}\hat{R}_{ss}\right],$$

where $\hat{R}_{ss} = \frac{1}{M}\sum_{k=1}^{M} S_k^T S_k$.

Assume R_{yy} can be expanded into its eigenvalues and eigenvectors decomposition $R_{yy} = \sum_{i=1}^{Q} \lambda_i u_i u_i^T$, then R_{nn} can be written as $R_{nn} = \sum_{i=1}^{Q} R_{nn}(0) u_i u_i^T$, and the inverse of $R_{nn}(0)I + R_{yy}$ is given by

$$(R_{nn}(0)I + R_{yy})^{-1} = \frac{1}{R_{nn}(0)}\left[I - \sum_{i=1}^{Q}\frac{\lambda_i}{R_{nn}(0) + \lambda_i} u_i u_i^T\right],$$

where Q is the rank of R_{yy}.

Therefore,

$$tr\left[(R_{nn}(0)I + R_{yy})^{-1}\hat{R}_{ss}\right] = \frac{1}{R_{nn}(0)}\left[tr(\hat{R}_{ss}) - \sum_{i=1}^{Q}\frac{\lambda_i}{R_{nn}(0) + \lambda_i} u_i^T \hat{R}_{ss} u_i\right],$$

and

$$|R_{nn}(0)I + R_{yy}| = [R_{nn}(0)]^{P-Q}\prod_{i=1}^{Q}(R_{nn}(0) + \lambda_i) .$$

Thus, the likelihood function $\Phi(S/R_{nn}(0), \lambda_i, u_i)$ can be rewritten as

$$\Phi = (P-Q)\ln R_{nn}(0) + \sum_{i=1}^{Q}\ln(R_{nn}(0) + \lambda_i) + \frac{1}{R_{nn}(0)}\left[tr(\hat{R}_{ss}) - \sum_{i=1}^{Q}\frac{\lambda_i}{R_{nn}(0) + \lambda_i}u_i^T\hat{R}_{ss}u_i\right].$$

Till now we can estimate three variables $R_{nn}(0), \lambda_i, u_i$ step by step through minimizing Φ with respect to only one variable and with other variables fixed.

A.2 Estimation of $u_i, \lambda_i, R_{nn}(0)$

We first need to find estimation of u_i, which minimizes Φ with $\lambda_i, R_{nn}(0)$ fixed. The minimization here is equivalent to maximizing the quantity $\sum_{i=1}^{Q}\frac{\lambda_i}{R_{nn}(0) + \lambda_i}u_i^T\hat{R}_{ss}u_i$. Since $u^T\hat{R}_{ss}u$ is maximum if u is the eigenvector of $\hat{R}_{ss}$ corresponding to the largest eigenvalue, the sum of Q quadratic forms reaches maximum if u_i takes on $\sigma_i (i \in [1, Q])$, which are the eigenvalues of $\hat{R}_{ss}$ arranged in decreasing order.

Noting that $tr(\hat{R}_{ss}) = \sum_{i=1}^{P}\sigma_i$ and $\frac{\lambda_i}{R_{nn}(0) + \lambda_i} = 1 - \frac{R_{nn}(0)}{R_{nn}(0) + \lambda_i}$. Thus the minimum of function Φ is given by

$$\begin{aligned}\Phi &= (P-Q)\ln R_{nn}(0) + \sum_{i=1}^{Q}\ln(R_{nn}(0) + \lambda_i) + \frac{1}{R_{nn}(0)}\left[tr(\hat{R}_{ss}) - \sum_{i=1}^{Q}\frac{\sigma_i\lambda_i}{R_{nn}(0) + \lambda_i}\right] \\ &= (P-Q)\ln R_{nn}(0) + \sum_{i=1}^{Q}\ln(R_{nn}(0) + \lambda_i) + \frac{1}{R_{nn}(0)}\sum_{i=Q+1}^{P}\sigma_i + \sum_{i=1}^{Q}\frac{\sigma_i}{R_{nn}(0) + \lambda_i}.\end{aligned}$$

Second, we minimize Φ with respect to λ_i. Recall that the function is minimum for the gradient equal to zero and the hessian positive. The gradient equals zero when

$$\frac{1}{R_{nn}(0) + \lambda_i} - \frac{\sigma_i}{(R_{nn}(0) + \lambda_i)^2} = 0, 1 \le i \le Q,$$

which gives

$$\hat{\lambda}_i = \sigma_i - R_{nn}(0) .$$

The minimum of the function Φ assumes the form

$$\Phi = (P-Q)\ln R_{nn}(0) + \sum_{i=1}^{Q} \ln(\sigma_i) + \frac{1}{R_{nn}(0)} \sum_{i=Q+1}^{P} \sigma_i + Q .$$

Third, the function Φ is minimum with respect to $R_{nn}(0)$ for

$$\frac{P-Q}{R_{nn}(0)} - \frac{1}{(R_{nn}(0))^2} \sum_{i=Q+1}^{P} \sigma_i = 0 ,$$

so, the estimation of $R_{nn}(0)$ is given by

$$\hat{R}_{nn}(0) = \frac{1}{P-Q} \sum_{i=Q+1}^{P} \sigma_i ,$$

and the function Φ can be rewritten as

$$\Phi(Q) = (P-Q)\ln\left[\frac{1}{P-Q}\sum_{i=Q+1}^{P}\sigma_i\right] - \sum_{i=Q+1}^{P}\ln(\sigma_i) + P + \sum_{i=1}^{P}\ln(\sigma_i) .$$

A.3 Akaike criterion and estimation of Q, $R_{nn}(0)/R_{rr}(0)$

The Akaike estimate of the order of a model[15] is the minimum of the function

$$f(q) = \Phi(q) + \frac{num1}{num2} ,$$

where num1 is the number of free parameters, num2 is the number of observations, and $\Phi(q)$ is the likelihood function of the model of order q. In our case, with the constant term being removed, the function $f(q)$ takes the following form

$$f(q) = (P-q)\ln\left[\frac{1}{P-q}\sum_{i=q+1}^{P}\sigma_i\right] - \sum_{i=q+1}^{P}\ln(\sigma_i) + q(P+0.5-q) .$$

So, the estimation of Q is q with which the function reaches its minimum.

Because of the equality of Eq. 2.42, the eigenvalue λ_i and α_i are linked together by

the relation

$$\lambda_i = R_{rr}(0)\,\alpha_i$$

with α_i as the eigenvalues of the correlation matrix R_{ww}. So, we estimate $R_{rr}(0)$ by means of

$$\hat{R}_{rr}(0) = \frac{\sum_{i=1}^{Q}\left(\frac{\lambda_i}{\alpha_i}\right)}{Q}.$$

Finally, the estimation of $R_{nn}(0)/R_{rr}(0)$ is given by

$$\frac{\hat{R}_{nn}(0)}{\hat{R}_{rr}(0)} = \frac{Q}{(P-Q)} \times \frac{\sum_{i=Q+1}^{P} \sigma_i}{\sum_{i=1}^{Q}\left(\frac{\lambda_i}{\alpha_i}\right)}.$$

References

[1] OPPENHEIM,A.V., KOPEC,G.E. and TRIBOLET,J.M. Signal Analysis by Homomorphic Prediction. IEEE Transactions on Acoustics, Speech and signal Processing, 24, 1976:327-332.

[2] RICE, R.B. Inverse Convolution Filters, 27, 1662:4-18

[3] ROBINSON, E.A. Multichannel Z-Transforms and Minimum Delay. Geophysics, 31, 1966:473-500.

[4] ROBINSON, E.A. and TREITEL, S. Principles of Digital Wiener filtering. Geophysical Prospecting, 15, 1967:311-333.

[5] OPPENHEIM,A.V. Superposition in a Class of Non-Linear Systems, TR-432. Cambridge, MA, MIT, 1965.

[6] NICOLAS, P. Deconvolution by Homomorphic and Wiener filtering. U.S. Dept. of Commerce National Technical Information Service, Springfield, VA. 22161

[7] OPPENHEIM,A.V., SCHAFER, R.W. Discrete-Time Signal Processing, Prentice Hall, 1989.

[8] TRIBOLET, J.M. Seismic Application of Homomorphic Signal Processing. Englewood Cliffs, NJ, Prentice-Hall, 1978.

[9] BHANU, B. and McCLELLAN, J.H. On the Computation of the Complex Cepstrum. IEEE transactions on Acoustics, Speech and Signal Processing, 28, 1980:583-585.

[10] BHANU, B. Computation of the Complex Cepstrum (thesis), Cambridge, MA, MIT, 1977

[11] VAN TRESS, H.L.Detection, Estimation and Modulation Theory, part I. New York, NY, Wiley, 1968.

[12] JEAN OK NAM, Signal Recovery Using Cepstrum Smoothing in the Shallow Water Environment, MS thesis, Massachusetts Institute of Technology, 1994.

[13] JURKEVICS, A. and WIGGINS, R. A Critique of Seismic Deconvolution Methods. Geophysics, 49, 1984:2109-2116.

[14] PAPOULIS, A. Probability, Random Variables, and Stochastic Processes, McGraw-Hill, 1991.

[15] AKAIKE, H.A. A New Look at the Statistical Model Identification. In: CHILDERS, D.G., ed. Modern Spectrum Analysis. Piscataway, NJ, IEEE Press, 1978:pp.234-241.